

Resilience of modern power distribution networks with active coordination of EVs and smart restoration

Alghamdi, Abdullah Ali M.; Jayaweera, Dilan

DOI:
[10.1049/gtd2.13002](https://doi.org/10.1049/gtd2.13002)

License:
Creative Commons: Attribution (CC BY)

Document Version
Publisher's PDF, also known as Version of record

Citation for published version (Harvard):
Alghamdi, AAM & Jayaweera, D 2023, 'Resilience of modern power distribution networks with active coordination of EVs and smart restoration', *IET Generation, Transmission and Distribution*, vol. 17, no. 21, pp. 4677-4906. <https://doi.org/10.1049/gtd2.13002>

[Link to publication on Research at Birmingham portal](#)

General rights

Unless a licence is specified above, all rights (including copyright and moral rights) in this document are retained by the authors and/or the copyright holders. The express permission of the copyright holder must be obtained for any use of this material other than for purposes permitted by law.

- Users may freely distribute the URL that is used to identify this publication.
- Users may download and/or print one copy of the publication from the University of Birmingham research portal for the purpose of private study or non-commercial research.
- User may use extracts from the document in line with the concept of 'fair dealing' under the Copyright, Designs and Patents Act 1988 (?)
- Users may not further distribute the material nor use it for the purposes of commercial gain.

Where a licence is displayed above, please note the terms and conditions of the licence govern your use of this document.

When citing, please reference the published version.



Take down policy

While the University of Birmingham exercises care and attention in making items available there are rare occasions when an item has been uploaded in error or has been deemed to be commercially or otherwise sensitive.

If you believe that this is the case for this document, please contact UBIRA@lists.bham.ac.uk providing details and we will remove access to the work immediately and investigate.

ORIGINAL RESEARCH

Resilience of modern power distribution networks with active coordination of EVs and smart restoration

Abdullah Ali M. Alghamdi^{1,2}  | Dilan Jayaweera¹ 

¹Department of Electronic, Electrical and Systems Engineering, School of Engineering, University of Birmingham, Birmingham, UK

²Department of Electric Engineering, School of Engineering, Taibah University, Yanbu, KSA

Correspondence

Abdullah Ali M. Alghamdi and Dilan Jayaweera, Department of Electronic, Electrical and Systems Engineering, School of Engineering, University of Birmingham, Birmingham, UK.

Email: axa1455@student.bham.ac.uk and d.jayaweera@bham.ac.uk

Funding information

Taibah University; University of Birmingham

Abstract

In this modern era of cyber–physical–social systems, there is a need of dynamic coordination strategies for electric vehicles (EVs) to enhance the resilience of modern power distribution networks (MPDNs). This paper proposes a two-stage EV coordination framework for MPDN smart restoration. The first stage is to introduce a novel proactive EV prepositioning model to optimize planning prior to a rare event, and thereby enhance the MPDN survivability in its immediate aftermath. The second stage involves creating an advanced spatial–temporal EV dispatch model to maximize the number of available EVs for discharging, thereby improving the MPDN recovery after a rare event. The proposed framework also includes an information system to further enhance MPDN resilience by effectively organizing data exchange among intelligent transportation system and smart charging system, and EV users. In addition, a novel bidirectional geographic graph is proposed to optimize travel plans, covering a large penetration of EVs and considering variations in traffic conditions. The effectiveness is assessed on a modified IEEE 123-node test feeder with real-world transportation and charging infrastructure. The results demonstrate a significant improvement in MPDN resilience with smart restoration strategies. The validation and sensitivity analyses evidence a significant superiority of the proposed framework.

1 | INTRODUCTION

Power distribution networks are crucial for ensuring a reliable electricity supply to consumers, and their resilience during rare events is key. Thus, it is necessary to develop robust methodologies to guarantee efficient restoration of supply, minimizing any load outage periods to reduce the resulting economic and societal impacts [1–3]. This paper explores integrating technological advancements in intelligent transportation systems (ITSs) and smart charging stations (SCSs) into modern power distribution networks (MPDNs) to develop smart and resilience-oriented restoration strategies. The relatively recent widespread adoption of electric vehicles (EVs) and associated charging points (CPs) has introduced opportunities in this era, albeit subject to novel challenges. Integrating EVs and CPs into the existing resilience framework would provide additional mobile power sources (MPSs) to support restoration efforts, thereby improv-

ing resource utilization to help facilitate a coordinated response to power demand fluctuations. However, the integration of EVs and CPs poses challenges in terms of optimization positioning, routing, and power scheduling [4]. Optimizing critical pathways for high penetration of EVs is a complex process, due to the potential for high congestion rates (CRs) and road damage in the aftermath of rare event, when locating an available charging infrastructure becomes more difficult. To address these challenges and leverage the opportunities presented by EVs, effective EV coordination strategies can be developed to manage prepositioning and dispatching [5]. Such strategies would play a vital role in ensuring the efficient restoration of MPDNs enhancing their resilience in the face of severe disruption. Therefore, this paper aims to provide a comprehensive EV coordination framework integrating the emerging technologies of ITS and SCS to harness the potential of EVs and CPs to improve the resilience of MPDN.

This is an open access article under the terms of the [Creative Commons Attribution](https://creativecommons.org/licenses/by/4.0/) License, which permits use, distribution and reproduction in any medium, provided the original work is properly cited.

© 2023 The Authors. *IET Generation, Transmission & Distribution* published by John Wiley & Sons Ltd on behalf of The Institution of Engineering and Technology.

1.1 | Motivation

An effective framework for coordinating EVs is crucial to enhance the MPDN resilience, due to the huge volume of data detailing the motion and other vital aspects of EVs. Such a framework can be realized by integrating MPDN, SCS, and ITS [6–8]. The Internet of Things (IoT) and fifth-generation (5G) network technologies expedite communication between ITS/SCS automated systems and EVs, enabling coordination via vehicle-to-everything (V2X) operation mode across newly implemented machinery (e.g. roadside unit [RSU] and CPs) to support vehicular communications [9, 10]. Incorporating these technologies enables ITS/SCS automated systems and the MPDN operator to both store information pertaining to EVs, roads, and CPs across distributed data centres (DDCs), and simultaneously update resilience-oriented restoration plans of roads, CPs, and the MPDN components in real-time [11]. The advent of cyber–physical–social systems also facilitates data exchange from EVs through an efficient information system [1, 12], which is of particular relevance to the MPDN restoration, and considered desirable by power utilities seeking to improve the MPDN resilience during high-impact low-probability events (i.e. rare events).

It is important to note here that rare events can destroy transportation systems, roads and CPs, which would then impact the dispatching of EVs, exacerbating difficulties with service restoration and compromising the MPDN resilience. The literature to date focused on coupling MPDN branches and transportation for emergency mobile power source dispatching problems, while neglecting geographic factors such as actual locations, distance, energy consumption rates, road congestion and damage status, as well as CPs' capacity, characteristics, and technologies. Although there has been progress deploying constraints relating to transportation roads in [13–15], current research studies examine dispatching problems consider transportation and charging station systems in a deterministic manner. Such an approach does not thoroughly address the full impact of interrelated geographic and spatial-temporal positioning and dispatching constraints on the ITS, or the SCS, in reference to its potential role in enhancing the MPDN resilience after a rare event.

1.2 | Literature review

EVs play a crucial role in enhancing the MPDNs' resilience by serving as MPSs with the capacity to navigate transportation systems and use distributed smart CPs [6, 16]. This is especially true in areas with a high penetration of EVs and sufficient CPs [16, 17]. The utilization of different types of MPSs has previously been examined when evaluating resilience-oriented restoration strategies that support the MPDN outage load. In [18], a two-stage restoration scheme is proposed to enhance the resilience of MPDNs during emergencies. The routing and scheduling of MPSs is thus optimized in coordination with dynamic network reconfiguration. However, the practical deployment and coordination of MPSs may result in challenges,

such as limited power availability and an inadequate charging infrastructure for EVs. In [15], a dynamic load restoration method is proposed to effectively restore service in MPDNs by managing interdependence within the transportation system. However, mobile emergency generators (MEGs) may not necessarily be uniform, impacting their effectiveness. Therefore, additional testing and refinement are necessary to execute this method in real-world scenarios. In [19], a time–space network is utilized to optimize the routing of flexible emergency MPSs for MPDN restoration. A transportation network simplification method is proposed to reduce the number of binary variables involved in the optimization process, while simultaneously enhancing the optimality of the routing decisions obtained, and reducing the computational burdens arising from calculation. However, the lack of an existing functional charging infrastructure for mobile energy storage systems (MESSs) complicates the transportation network simplification method, necessitating more nodes and binary variables. In [20–22], a joint restoration model is proposed to enhance post-disaster resilience by coordinating electric bus scheduling with MPDN restoration. The objectives here are to maximize load pickups and minimize electric bus rental expenses. However, assumptions concerning charging station availability and the bus companies' willingness to participate may not represent real-world implementations accurately. Moreover, it is important to consider the additional restoration costs that arise when involving electric buses and companies; that is, the cost of charging the buses and the cost of compensating participating bus companies.

In [13, 23], the authors propose a rolling optimization framework for MESSs, which effectively optimizes the allocation and scheduling of MESSs, microgrids, and MPDN reconfiguration to restore critical loads during extreme events. However, these approaches simplify the distribution network and transportation system, ignoring real world constraints, such as the availability of CPs and road closures that affect movement of MPSs. In contrast, the authors in [24, 25] propose innovative approaches to reduce peak loads in grid connected photovoltaic-powered EV charging stations using coordinated controls. These approaches utilize real-time meteorological and load demand data to optimize EV charging, lowering peak power demand. However, further improvements to the proposed coordination and optimization of EVs are needed, particularly to maximize the utilization of CPs and to reduce peak loads for the duration of the cold load pick-up phenomenon that occurs after rare events.

Additionally, it is noteworthy that the utilization of MPSs to enhance the resilience of MPDNs is limited by their utility and reliance on prior knowledge to determine the probabilities for outages and affected areas. Therefore, it is important to note that they may not be sufficient to resolve unexpected outages when larger areas are affected, resulting in extended outages and disruptions. Existing studies have also highlighted the need for innovative frameworks to optimize coordinated utilization of EVs and CPs. While some promising approaches have been proposed, there remains a need to develop more comprehensive strategies to integrate the complexities of transportation networks, as well as the availability of CPs and other real-world constraints in optimization models. In addition, the

requirement for an intelligent coordination framework to organize high penetration EVs results in inefficient use of resources. Increased EV penetration also complicates transportation and charging station automated system prepositioning plans and dispatch strategies. This necessitates more sophisticated and smarter restoration strategies, to ensure EVs can access charging stations efficiently without triggering further disruption.

1.3 | Major contributions

To address the aforementioned challenges and further enhance MPDN resilience, an innovative resilient EV coordination framework with a novel proactive prepositioning model and an advanced spatial-temporal dispatching model is proposed here, with the aim of effectively bridging the coordination gap where there is penetration of EVs.

A novel information system is also proposed to further enhance the MPDN resilience by exchanging EV data among the MPDN operators, the automated ITS, automated SCS, and EV users. The methodology uses real traffic data and patterns to simulate a typical EV user behaviour in the real world.

Furthermore, a novel bidirectional geographic graph (BGG) is proposed to dynamically consider spatiotemporal factors, such as actual distance, traffic conditions, charging station availability, and power demand, to optimize routes between CPs and EVs accordingly. This helps reduce the load on the SCS to prevent overloading and queuing, which could lead to power outages and other disruptions.

1.4 | Paper organization

This paper is structured as follows: Section 2 presents the problem statement and the proposed information system. Section 3 provides the mathematical formulations for the proposed EV coordination framework. Section 4 covers the solution, method and linearization. Section 5 presents details of the simulation studies and tests the systems' specifications. Section 6 provides the simulation results and discusses the proposed EV coordination framework. Section 7 covers the validation and sensitivity analysis for the model proposed here. Section 8 provides further remarks on the proposed work. Section 9 concludes the article. The Appendix presents the remaining mathematical formulations and figures adapted.

2 | EVS COORDINATION FRAMEWORK

2.1 | Problem statement

A modified conceptual resilience curve (R) is presented in Figure 1 to illustrate the variance in the MPDN robustness levels during pre-disruption ($t_0 \sim t_e$), disruption progress ($t_e \sim t_{pe}$), and the restorative phases ($t_{pe} \sim t_{pr}$) of a rare event [26]. The comparison highlights the superiority of the proposed intelligent EV coordination framework (i.e. dashed line) over

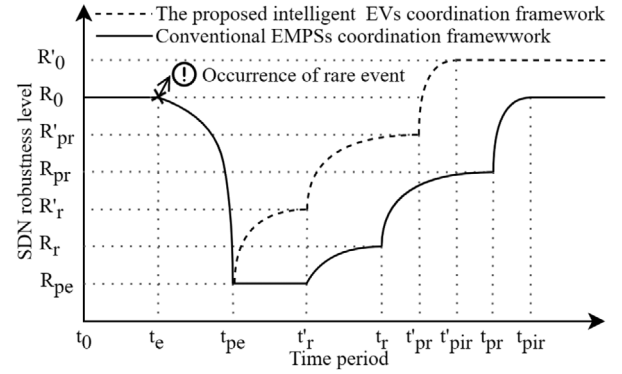


FIGURE 1 A modified conceptual resilience curve associated with an event [26].

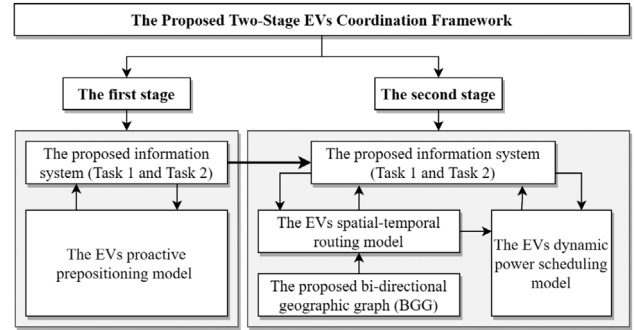


FIGURE 2 The proposed two-stage electric vehicle (EV) coordination framework and associated models.

the conventional EMPS coordination framework (i.e. solid line). Accordingly, two categories of measures are employed to enhance the MPDN resilience: for example, planning oriented measures prior to the event ($t_0 \sim t_e$) in the initial stage, and operation-oriented measures after the event ($t_{pe} \sim t_{pr}$) in the second stage. Figure 2 demonstrates these stages, including the models proposed to enhance the resilience of MPDN.

In the first stage, MPDN survivability is evaluated from t_{pe} to t_r , proving the ability of the proposed EV prepositioning model to enhance MPDN resilience from R_r to R'_r at an earlier time (t'_r) before t_r . The MPDN reconfiguration model is co-optimized to shift the system into a state where it is less impacted and stressed by the event [27]. In the initial stage of the EV coordination framework, EV prepositioning at the CPs is carried out to ensure prompt discharging of connected EVs immediately after a rare event occurrence. Additionally, the MPDN operator and the automated ITS/SCS gather and update data associated to EVs, CPs, roads, and the MPDN. Consequently, this active data collection and updating contribute to the effective enhancement of MPDN resilience for the subsequent stage. The enhancement is achieved through the optimization of well-informed restorative decisions.

In the second stage, MPDN recovery is measured from t_r to t_{pir} proving the capability of the proposed EV dispatching model to enhance MPDN resilience from R_{pr} to R'_{pr} , achieving complete restoration at t'_{pir} and enhancing the MPDN

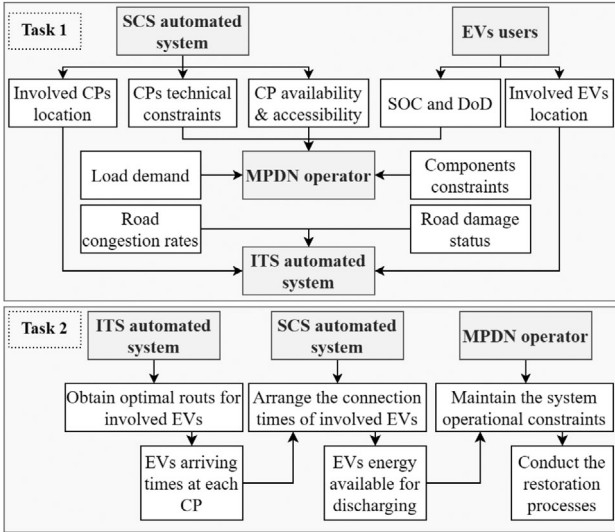


FIGURE 3 The proposed information system.

robustness level from R_0 to R'_0 . At this stage, spatiotemporal routing and dynamic power scheduling of EVs, dynamic network reconfiguration and dynamic power dispatch of the MPDN are co-optimized. Consequently, the proposed EVs coordination framework enhances the MPDN resilience from the solid curve, shown in Figure 1, to the dashed curve. The decisions and data obtained and collected during the first stage are updated in this stage, ensuring a continuous process of updates to guarantee the most optimal restorative decisions. This includes routing decisions that require positioning and routing EVs to CPs across critical routes, at the same time, involves power scheduling decisions that necessitate a gradual restoration of the MPDN within a shorter time frame, thereby avoiding any further disruption or collapse.

2.2 | Information system

As stated above, the aim of the proposed information system is to further enhance the resilience of the MPDN by effectively organizing data exchange among the MPDN operators, the ITS and SCS automated systems, and EV users. In Figure 3, the information system is divided to perform two tasks (i.e. *Task 1* and *Task 2*), each according to a systematic order. During *Task 1*, each entity collects and shares the necessary data, as indicated by the arrows. This ensures the automated systems have access to the routing plan for the EVs across the roads, as well as to the connection and discharging schedule at CPs during *Task 2*. This data exchange is conducted in coordination with the MPDN operators, so as to ensure outage loads are survived and are restored efficiently, maintaining the operational constraints of the grid components. Specifically, automated ITS ensures optimal critical routes for each EV to reach its designated CP, while the automated SCS schedules the connection between the EVs and the CPs. Additionally, the automated SCS optimizes the utilization of CPs throughout the restoration period, enabling the

most effective use of charging infrastructures and contributing to faster and more efficient restoration of the MPDN.

This paper assumes the data obtained and shared by the ITS/SCS automated system in the first and second tasks is automatically transmitted to DDCs via RSUs within the intelligent transportation infrastructure [28]. Thus, the MPDN operators and the ITS/SCS automated system dynamically update the MPDN resilience-oriented restoration plan at each predefined time point. Moreover, the ITS/SCS automated systems share data with the EVs via V2X operating modes [29]; particularly, vehicle-to-infrastructure (V2I) communications [30].

The data exchange depicted in Figure 3 is used in both stages of the proposed EV coordination framework. The communication operations shown are continuously updated at every time step (Δt) throughout the restoration time horizon (\mathcal{T}). This ensures the restoration process remains synchronized and efficient. To maintain clarity, *Task 1* represents the proposed communication protocol between the associated entities for data exchange and updates. In contrast, *Task 2* represents the communication protocol between entities for initiating restorative actions, which includes the models proposed here for EV prepositioning, routing, and dispatching. Both tasks are performed simultaneously and form the layout of the information system, which is integrated into the first and the second stages of the proposed EV coordination framework, as described below:

2.2.1 | The first stage

In the first stage of the proposed EVs coordination framework, two key operations are conducted: EV prepositioning and planning for the restorative phase. During EV prepositioning, the MPDN operator and the ITS/SCS automated system take preventive action to enhance the MPDN resilience. The automated SCS collects technical and geolocation information about the V2G-CPs and C-EVs, maximizing utilization of the available EVs for post-event operations. This is illustrated as *Task 1* in Figure 3. These EVs are prepositioned to participate and discharge shortly after the rare event, as indicated in *Task 2*. In addition, the automated ITS plans for the restorative phase by collecting location and technical data about T-EVs, as indicated in *Task 1* in Figure 3. This information is utilized to optimize the critical route for each T-EV once road damage status and traffic conditions are obtained shortly after the event, during *Task 2*. Meanwhile, the MPDN operator maximizes survived loads while maintaining requisite constraints upon network components. For example, as shown in Figure 4a, the automated SCS collects technical data regarding V2G-CPs, C-EV6, and C-EV5, while T-EV1 and T-EV2 are being pre-positioned. However, T-EV3 is not eligible for pre-positioning due to its low average state of charge ($SOC_{e,t}^{av}$) level.

2.2.2 | The second stage

In the second stage of the proposed EV coordination framework, the focus shifts to dispatching EVs according to the

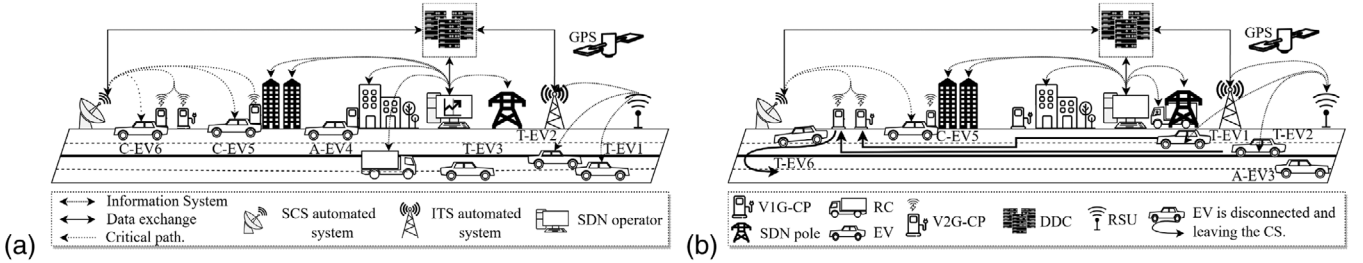


FIGURE 4 An illustration of the proposed electric vehicle (EV) coordination framework. (a) Preventive actions associated with the first stage (before the event $[t_0 \sim t_{pe}]$). (b) Restorative actions associated with the second stage (after the event $[t_{pe} \sim t_{pr}]$).

preparatory actions taken in the first stage. During EV dispatch, several key operations are conducted using information collected during the first stage. Notably, this information is repeatedly updated at every time step (Δt) on the restoration time horizon (\mathcal{T}). The automated SCS reports the damage status of V2G-CPs and updates the available energy of C-EVs ($SOC_{e,t}^{ar}$), as depicted in *Task 1* in Figure 3. It ensures that C-EVs are immediately disconnected if the level of their state of charge (SOC_e) reaches the minimum boundary (\underline{SOC}_e). This allows the next T-EV in the queue to participate immediately, minimizing queues and maximizing use of CPs during *Task 2*. Simultaneously, the automated ITS constantly updates traffic data, road status, and CRs at each time step during *Task 1*. This information is utilized to dynamically optimize the critical pathways for T-EVs in *Task 2*, thereby ensuring efficient and timely routing decisions. Furthermore, the MPDN operator keeps track of network components' status based on the reports provided by repair crews (RCs). This enables them to update the status of network components accordingly. For example, Figure 4b illustrates the disconnectedness of C-EV6, allowing T-EV2 to connect and discharge. The automated ITS shares optimal routes between V2G-CPs and T-EV1/T-EV2, while C-EV5 is actively discharging.

2.3 | Algorithm

The innovative algorithm in this section asserts that EVs and CPs must not deviate from their prepositioning and dispatching plans, as determined by the ITS/SCS automated systems and the MPDN operators according to the proposed information system set out in Section 2.2. This is achieved by modelling binary variables ($x_{e,t}$), ($x_{cp,t}$), and ($x_{e,cp,t}$), in which they are explained in this section, respectively. The flowchart in Figure 5 illustrates the proposed algorithm.

For the former variable ($x_{e,t}$), EVs are categorized according to their connection mode: First, the away EV (A-EV), which refers to an EV that cannot participate in the restoration process, due to being connected to a unidirectional CP, and/or its state-of-charge level (SOC_e) being equal to or lower than the minimum value (\underline{SOC}_e). Here, $x_{e,t} = 0\forall t$. Second, the connected EV (C-EV), which refers to an EV that can participate in the restoration process, since it is connected to a bidirectional CP and its SOC_e is greater than \underline{SOC}_e . Here, $x_{e,t} = 1\forall t \Rightarrow$

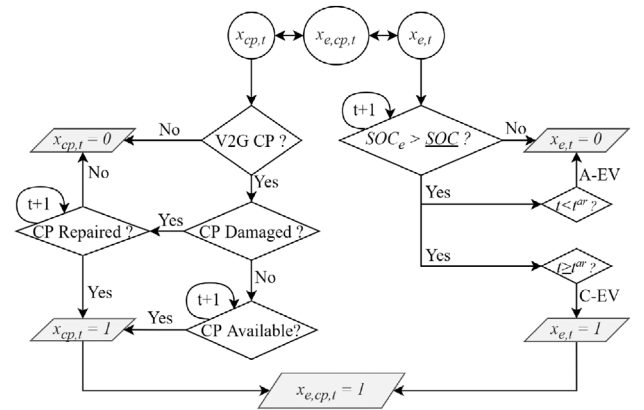


FIGURE 5 Flowchart for the proposed algorithm.

$SOC_e \geq \underline{SOC}_e$. Third, the travelling EV (T-EV), which refers to an EV that is travelling and cannot connect until its arrival time ($t_{e,cp}^{ar}$) is reached, where $t = t_{e,cp}^{ar}$. To enable participation, T-EV calculated SOC_e at $t_{e,cp}^{ar}$ must be greater than \underline{SOC}_e . Here, $x_{e,t} = 1, t \geq t_{e,cp}^{ar} \Rightarrow SOC_e \geq \underline{SOC}_e$.

For the medial variable ($x_{cp,t}$), CPs are classified by technology into two categories. First, the bidirectional CP (V2G-CP) which operates a CP support vehicle-to-grid (V2G) operation mode, for example, a vehicle-to-building (V2B) operation mode, which can inject the power to the MPDN allowing C-EV to discharge. Moreover, various capacities (i.e. the characteristics of supplying electric power to an EV, ranging from slow to ultrarapid) and capabilities (i.e. the constraint of charging slot allows for connection to only one EV at each time period $[t_n \sim t_{n+\tau}]$, given τ is the connection period of time) of V2G-CPs are considered. Here, $x_{cp,t} = 1\forall t$, if it is not damaged, and 0 otherwise. Second, a unidirectional CP (V1G-CP) that is a CP cannot inject power back to the MPDN: for example, in the vehicle-to-home (V2H) operation mode. Here, $x_{cp,t} = 0\forall t$.

For the latter variable ($x_{e,cp,t}$), if a C-EV is connected to V2G-CP, it is equal to 1 for the duration of the connection period ($t_{e,cp}^{ar} \leq t \leq \tau$), and 0 otherwise. Consequently, charging/discharging processes, connecting and disconnecting timings, and routes and destinations comply with the obtained EV prepositioning and dispatching plan for the ITS/SCS automated systems.

3 | MATHEMATICAL FORMULATION

3.1 | Proactive repositioning of EVs

Before a rare event occurs, the MPDN operator and ITS/SCS automated systems collaborate to maximize the number of connected EVs so as to enhance MPDN survivability. The objective function of the first stage, in (1), maximizes the amount of survived MPDN loads at $t = 0$.

$$\min(\max_{e, cp, t} \sum_l \sum_{\phi} [x_{l, \phi, t}^L \cdot P_{l, \phi, t}^L]), \quad (1)$$

$$\forall l \in \mathcal{L} \subset \mathcal{K}, e \in \mathcal{Y} \subset \mathcal{K}, cp \in \mathcal{Y} \subset \mathcal{K}, \phi \in \Phi, t = 0$$

Unlike [13–15, 18, 20–23, 31–37], the number of available EVs is not predetermined here. Thus, the objective function facilitates the prompt discharge of available EVs following the event to maximize the amount of restored load in the inner level, while obviating the necessity for further EV discharge if all loads are survived in the outer level. By involving the variables at the outer level, constraint (2) is modelled using charging status ($x_{e,t}^{ch}$) and discharging status ($x_{e,t}^{disch}$), as well as binary variables to ensure the EVs are repositioned and connected at predetermined CPs to allow them to start discharging immediately after the event. Constraint (3) maintains the capability of CPs:

$$x_{e,t}^{ch} + x_{e,t}^{disch} \leq x_{e, cp, t}, \forall e \in \mathcal{G}^E, cp \in \mathcal{N}^{CP}, t = 0, \quad (2)$$

$$\sum_e x_{e,t} \leq x_{cp, t}, \forall e \in \mathcal{G}^E, cp \in \mathcal{N}^{CP}, t = 0. \quad (3)$$

The problem of repositioning is intelligently addressed in the proposed approach by utilizing variables integrated into the second stage of the framework. This approach makes the proposed method novel and highly effective as means of improving the resilience of the MPDN. This is because the proposed repositioning model allows for the transfer of updated initial values for decision variables, via the information system to the second stage of EVs dispatching, as shown in Figure 2. Consequently, the information system, as described in Section 2.2, facilitates effective coordination between the MPDN operators and the ITS/SCS automated system. Moreover, this model effectively incorporates diverse categories of EVs and CPs into the algorithms proposed in Section 2.3. The proposed repositioning model also ensures the MPDN resilience continues to improve shortly after the disaster, thereby maximizing survived loads. In the second stage, it enhances initial dispatch decisions to maximize restored load.

The inner level of the objective function is subjected to the following constraints:

$$\begin{aligned} V_{i, \phi, t} - V_{j, \phi, t} &\leq \tilde{z}_{ij, \phi} S_{ij, \phi, t}^* + \tilde{z}_{ij, \phi}^* S_{ij, \phi, t} \\ + M \left(1 - x_{i, \phi, t}^N \right), &\forall ij \in \mathcal{B}/\mathcal{V}, \phi \in \Phi, t = 0, \end{aligned} \quad (4)$$

$$\begin{aligned} V_{i, \phi, t} - V_{j, \phi, t} &\geq \tilde{z}_{ij, \phi} S_{ij, \phi, t}^* + \tilde{z}_{ij, \phi}^* S_{ij, \phi, t} \\ - M \left(1 - x_{i, \phi, t}^N \right), &\forall ij \in \mathcal{B}/\mathcal{V}, \phi \in \Phi, t = 0, \end{aligned} \quad (5)$$

$$\begin{aligned} \left(\underline{V}_{i, \phi, t} \right)^2 V_{i, \phi, t} &\leq V_{i, \phi, t} \leq \left(\overline{V}_{i, \phi, t} \right)^2 V_{i, \phi, t}, \\ \forall i, j \in \mathcal{V}, \phi \in \Phi, t &= 0, \end{aligned} \quad (6)$$

$$\begin{aligned} \sum_{ji} P_{ji, \phi, t}^B + P_{e, \phi, t}^{disch} &= \sum_{ij} P_{ij, \phi, t}^B + P_{e, \phi, t}^{ch} + P_{l, \phi, t}^L, \\ \forall e \in \mathcal{G}^E, \phi \in \Phi, t &= 0, \end{aligned} \quad (7)$$

$$\begin{aligned} \sum_{ji} Q_{ji, \phi, t}^B + Q_{e, \phi, t}^{disch} + Q_{v, \phi, t}^C &= \sum_{ij} Q_{ij, \phi, t}^B + Q_{l, \phi, t}^L, \\ \forall e \in \mathcal{G}^E, \phi \in \Phi, v \in \mathcal{V}, t &= 0. \end{aligned} \quad (8)$$

Since the MPDN is naturally unbalanced, the three-phase unbalanced power flow model is applied here [38–41]. First, constraints (4) and (5) represent the three-phase line model that ensures the feasible range of voltage difference between the two end nodes (i), and (j), in each line (i, j) and phase (ϕ) except for the voltage regulators and transformers. Note that $\tilde{z}_{ij, \phi} \in \mathbb{C}^{3 \times 3}$ is the equivalent three-phase line impedance matrix, consisting of constant values defined in [39]. The three-phase apparent power ($S_{ij, \phi, t}$) from node (i) to node (j) at time (t) is equivalent to $[P_{ij, a, t} + iQ_{ij, a, t}, P_{ij, b, t} + iQ_{ij, b, t}, P_{ij, c, t} + iQ_{ij, c, t}] \in \mathbb{C}^{3 \times 3}$. Note that, subscript “ i ” denotes the node index, while a complex number in the imaginary part is denoted as “ i ”. M is a large positive number and is selected to ensure constraints are valid only when the line is energized. Second, the regulators are assumed to be wye-connected, and the tap setting is continuous [42] and approximate as suggested in [43], using constraint (6) to force the regulators’ voltage on the secondary side of the voltage regulator to fall within 5% of the primary side. Constraints (7) and (8) are the three-phase active and reactive power node balance, respectively.

Furthermore, the mathematical formulations for the remaining MPDN operational constraints are presented in Equations (A.1)–(A.6) in the Appendix. These include the radiality constraint, active power limits for EV charging and discharging operations, and constraints on capacitor reactive power, line power, node voltages, and regulator voltages.

3.2 | Dynamic dispatch of EVs

After the occurrence of a rare event, damage to the MPDN components is addressed by the MPDN operator; concurrently, the automated ITS and automated SCS reports the status of roads and CPs, respectively. At this stage, extensive penetration of EVs is ordered to restore the maximum possible proportion

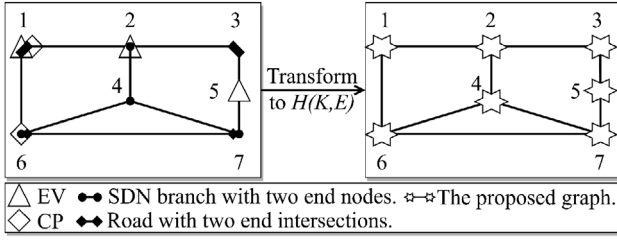


FIGURE 6 An illustration the proposed geographic graphs $\mathcal{H}(\mathcal{K}, \mathcal{E})$.

of the outage of the MPDN load as follows:

$$\begin{aligned} & \max \sum_t \left(\sum_{\phi} \sum_l [x_{l,t}^L \cdot P_{l,\phi,t}^L] \right. \\ & \left. - \sum_{cp} \sum_e \sum_r [D_{e,cp,r,t} \cdot ECR_e] \right), \end{aligned} \quad (9)$$

$$\begin{aligned} \forall l \in \mathcal{L} \subset \mathcal{K}, e \in \mathcal{Y} \subset \mathcal{K}, cp \in \hat{\mathcal{Y}} \subset \mathcal{K}, r \in \mathcal{R} \subset \mathcal{E}, \\ \phi \in \Phi, t \in \mathcal{T}. \end{aligned}$$

In (9), the first line maximizes the number of restored loads, ensuring each load is restored non-decreasingly and fully recovered, preventing the restored load from being shed again. The second line minimizes the energy used during the transportation of EVs, taking into account the energy consumption rate (ECR_e) and considering only critical routes to avoid the unnecessary travel of EVs, resulting in an additional deficit of energy. The objective function quantifies the MPDN resilience via optimal EVs routing and power scheduling maintaining the MPDN operational constraints, as presented in the following subsections, respectively.

3.2.1 | Spatial-temporal routing model

Considering the transportation system's geographic constraints, the road map is defined by a BGG ($\mathcal{Z}(\mathcal{Y}, \mathcal{R})$). For intersection set (\mathcal{Y}), each node ($y : (\gamma, \beta)$) is determined by its coordinate (i.e. longitude (γ) and latitude (β)). This set contains the coordinates for the CPs ($\hat{\gamma} : (\gamma, \beta) \in \hat{\mathcal{Y}}$), and EVs ($\check{\gamma} : (\gamma, \beta) \in \check{\mathcal{Y}}$). In the case, the ends of the road (r) in the set of edges (\mathcal{R}) are modelled as $(\gamma_\delta, \gamma_\zeta) \in \mathcal{R}$. Similarly, the MPDN is designed to function as a BGG ($\mathcal{G}(\mathcal{N}, \mathcal{B})$). In the set of buses (\mathcal{N}), the nodes are indexed by $i : (\gamma_i, \beta_i)$, and $j : (\gamma_j, \beta_j)$, and branches are indicated as $\mathcal{B} = \{(i : (\gamma_i, \beta_i), j : (\gamma_j, \beta_j)) | i, j \in \mathcal{N}; i \neq j\}$. Correspondingly, the aforementioned graphs are combined into the proposed BGG (\mathcal{H}), with a set of nodes (\mathcal{K}) and edges (\mathcal{E}). For the set of nodes/intersections (\mathcal{K}), the geographic graph (\mathcal{H}) is intelligently modelled. This reduces the overall number of nodes without any loss of associated coordinates. Accordingly, similar coordinates are merged, which in turn significantly reduces the overall computational burden of the proposed methodology. For example, two graphs are represented in Figure 6, demonstrating the aforementioned graphs and the proposed geographic graph. The number of intersec-

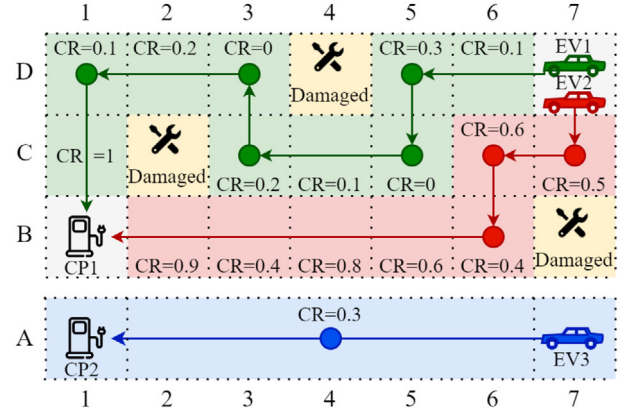


FIGURE 7 A demonstration of the proposed bidirectional geographic graph (BGG), illustrating travelling plans for EV1 and EV2 to CP1, as well as EV3 to CP2, for a single time step.

TABLE 1 The travelling information for the seismic routing plans of EV1, EV2, and EV3 in Figure 7.

From	To					
From EV	Cell	To CP	Cell	D^{tr}	t^{tr}	
EV1	C7	CP1	B1	10 pu	11.13 pu	5.85 pu
EV2	C7	CP1	B1	8 pu	12.54 pu	7.69 pu
EV3	A7	CP2	A1	6 pu	8.34 pu	3.76 pu

tions at *node1* is four (i.e. an EV, a CP, and the ends of two roads). However, these four intersections merge to become one node in $\mathcal{H}(\mathcal{K}, \mathcal{E})$. For the set of edges/segments (\mathcal{E}), combining the aforementioned graphs into the proposed graph increases the number of segments describing the associated edges ($\mathcal{E} = \{(k_\rho, k_\varrho) | k_\rho, k_\varrho \in \mathcal{K}; \rho \neq \varrho\}$). This in turn improves accuracy when calculating the actual distance between the EVs and CPs. For example, the edge ($k_3 \sim k_7$) in Figure 6 has become two segments (i.e. $k_3 \sim k_5$ and $k_5 \sim k_7$).

To enhance understanding and visualization of the improvements resulting from the integration of the proposed BGG into the routing models, Figure 7 illustrates three simplified routing examples. The figure assumes a distance of 1 p.u. between each pair of segments, assigning specific CR values to individual segments of the seismic road network. Additionally, Table 1 displays the routing information obtained from the simplified examples in Figure 7. In Table 1, the variables D^{tr} , t^{tr} , and SOC^{tr} represent the total travelled distance, total time required for travelling, and energy consumed for travelling, respectively. The routing plan for EV1 to CP1 represents the proposed routing model after integrating the BGG. As listed in Table 1, EV1 travelled further than EV2. However, EV1 arrived earlier and consumed less energy when travelling. This highlights the superior performance of the proposed routing model after integrating the BGG. By considering the variations in CRs across different road segments, the routing model can identify critical routes more effectively, ensuring earlier arrival and lower energy consumption, rather than solely focusing on distance.

Additionally, it is apparent that EV3 exhibits the lowest distance, travel time, and energy consumption compared to the other cases. This highlights the limitations of a deterministic approach reliant on the average CR of the entire route.

In a practical sense, relying exclusively on average CR does not accurately reflect the impact of real-world routing problems as experienced by typical EV users. Consequently, the MPDN operators may be vulnerable to risk of failure when effectively restoring outage loads. Note that the BGG is also designed to consider the dynamic variation in CRs for each time step (Δt), throughout the entire restoration period (\mathcal{T}). This supports accurate representation of real-world traffic conditions, allowing the automated ITS to make informed decisions based on current congestion levels.

Consequently, the proposed routing model not only exhibits advanced geographical capabilities to facilitate the coordination of high penetration of EVs on roads and CPs, but also includes dynamic updates accounting for a large volume of EV data that permits movement in multiple directions. This is achieved by introducing a bidirectional flow variable ($\tilde{x}_{k_\rho, k_\rho, e, t}$), which allows each EV to travel between node k_ρ and node k_ρ in either direction, mimicking typical EV driving behaviour in the real world. To ensure precise computation of the critical distance travelled by an EV (e) and its associated CO (cp), constraint (10) is introduced.

$$D_{k_\rho, k_\rho, e, t} = \sum_{k_\rho} \tilde{x}_{k_\rho, k_\rho, e, t} (D_{k_\rho, e, t} + (D_{k_\rho, k_\rho, e, t} \tilde{x}_{e, t}^{tr} CR_{r, t}^R)),$$

$$\forall (k_\rho, k_\rho) \in \mathcal{K}, (k_\rho, k_\rho) : (\gamma, \beta) = \check{\gamma} : (\gamma, \beta),$$

$$e \in \mathcal{G}^E, t \in \mathcal{T}, t + \tau \leq \mathcal{T}, \tau \leq t_{e, r}^{tr}, r \in \mathcal{E}. \quad (10)$$

This constraint represents a non-linear model designed to calculate the critical path distance ($D_{k_\rho, k_\rho, e, t}$) accurately. The variables $D_{k_\rho, e, t}$ and D_{k_ρ} are integrated to calculate the distance travelled by an EV e at time t to segment ends k_ρ and k_ρ , respectively. These segment ends are sequential and required for EVs to satisfy the travelling of the critical path. This ensures the EVs do not deviate from the critical path determined by the automated ITS.

The time variables related to the spatial-temporal routing model are formulated in Equations (11)–(16). These equations determine the limits on the travel time, connection time, discharging time, and disconnection time for the EVs included. The formulation of these time variables guarantees consistency with the other constraints and decision variables in the model. A visualization of these variables can be found in Figure 8. Accordingly, these variables are designed as follows:

$$t_e^{rq} = \{1, 2, \dots, \mathcal{T}\}, \forall e \in \check{\mathcal{Y}} \subset \mathcal{K}, t \in \mathcal{T} \quad (11)$$

$$t_e^{ar} = t_e^{rq} + t_e^{tr}, \forall e \in \check{\mathcal{Y}} \subset \mathcal{K}, t \in \mathcal{T} \quad (12)$$

$$t_e^w = t_e^{cn} - t_e^{ar}, \forall e \in \check{\mathcal{Y}} \subset \mathcal{K}, t \in \mathcal{T} \quad (13)$$

$$t_e^{cn} = t_e^{ar} + t_e^w, \forall e \in \check{\mathcal{Y}} \subset \mathcal{K}, t \in \mathcal{T} \quad (14)$$

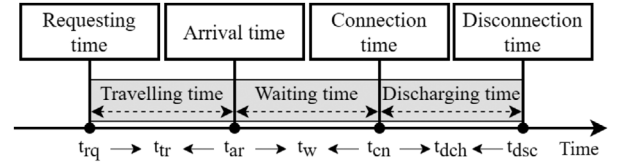


FIGURE 8 An illustration of requested time (t_e^{rq}), travelling time (t_e^{tr}), arriving time (t_e^{ar}), waiting time (t_e^w), connection time (t_e^{cn}), discharging time (t_e^{dch}), and disconnection time (t_e^{dsc}).

$$t_e^{dch} = \{SOC_{e, t}^{av} - DoD_e\} / P_{cp, t}^{discb}, \quad (15)$$

$$\forall e \in \check{\mathcal{Y}} \subset \mathcal{K}, cp \in \hat{\mathcal{Y}} \subset \mathcal{K}, t \in \mathcal{T}$$

$$t_e^{dsc} = t_e^{cn} + t_e^{dch}, \forall e \in \check{\mathcal{Y}} \subset \mathcal{K}, t \in \mathcal{T}. \quad (16)$$

In Equation (11), the integer positive parameter (t_e^{rq}) is proposed to indicate the participation request point in time for an EV (e); this reflects the order of the time step in the restoration processes (i.e. $\Delta t \in \mathcal{T}$). The time required for an EV (e) to travel from its location, captured at t_e^{rq} , to the designated CP (cp) is denoted as (t_e^{tr}). The arrival time variable (t_e^{ar}) in (12) indicates the point in time when the EV (e) arrives at the CP, and it is calculated by summing the requesting time (t_e^{rq}) and the travelling time (t_e^{tr}). Once an EV (e) has arrived at the designated CP, the waiting time variable (t_e^w) is calculated using Equation (13). This variable indicates the time period for an EV (e) to wait in the queue for the next availability in the CP. The calculation involves finding the difference between the arrival time (t_e^{ar}) and the connection time (t_e^{cn}).

In Equation (14), the connection time variable (t_e^{cn}) for an EV (e) is the sum of the arrival time (t_e^{ar}) and the waiting time (t_e^w). This variable indicates when the EV is connected to the CP and is ready to be discharged. The variable t_e^{cn} aligns with the time steps ($\Delta t \in \mathcal{T}$), which are predefined according to the proposed EV coordination framework time horizon (i.e. Section 4.1), facilitating synchronized and efficient coordination for timely restoration of the MPDN. When an EV (e) is connected to the designated CP, the time required to discharge the available energy ($SOC_{e, t}^{av}$) of the EV at the time of connection (t_e^{cn}) is denoted as (t_e^{dch}). This calculation determining of the discharging time variable is performed using Equation (15), which takes into account the rated discharging power ($P_{cp, t}^{discb}$) of the CP, and the depth of discharge (DoD_e) of the EV. Note that the discharge/charge rate of the EV ($P_{e, t}^{ch/discb}$) is also maintained as shown in Equations (A.16) and (A.17) in the Appendix. It is unnecessary to integrate ($P_{e, t}^{ch/discb}$), and the feasible limits into the time model, as the proposed algorithm here (i.e. Section 2.3) facilitates a connection between models. Accordingly, the disconnection time variable (t_e^{dsc}), as defined in Equation (16), indicates when an EV (e) will complete the discharging operation such that the designated CP becomes available for the next EV ($e + 1$) in the queue.

The remaining mathematical formulation in the proposed routing model is provided in Equations (A.7)–(A.10) in the

Appendix. These equations uphold the routing constraints to ensure compliance with the EVs' routing plan, maintaining the designated start and end intersections, enforcing the required travel distance for EVs, eliminating sub-tours, and calculating the critical path distance for each EV.

3.2.2 | Dynamic power scheduling model

In a practical sense, the amount of energy consumed ($SOC_{e,t}^{tr}$) by an EV (e) while travelling is relatively small. However, the proposed framework coordinates a large penetration of EVs, so the cumulative amount of $SOC_{e,t}^{tr}$ is considerable, affecting the resilience-oriented restoration strategy; hence, constraint (17) is used to calculate the available SOC level for the EVs:

$$SOC_{e,t}^{av} = SOC_{e,t-1}^{av} + \left(\eta^{CH} P_{e,t}^{ch} - \frac{P_{e,t}^{disch}}{\eta^{disch}} \right) \Delta t \quad (17)$$

$$-SOC_{e,t}^{tr}, \forall e \in \mathcal{G}^E, r \in \mathcal{R}, t \in \mathcal{T}.$$

Constraint (18) is a non-linear model computing the energy consumption while travelling on critical routes ($SOC_{e,t}^{tr}$), considering the energy consumption rate (ECR_e) for each EV (e) individually:

$$SOC_{e,t}^{tr} = x_{e,t}^{tr} ECR_e D_{k_\rho, k_\rho, e, t},$$

$$\forall e \in \mathcal{G}^E, t \leq t^{ar}, k_\rho, k_\rho \in \mathcal{K}, k_\rho : (\gamma, \beta) = \check{\gamma} : (\gamma, \beta), \quad (18)$$

$$k_\rho : (\gamma, \beta) = \hat{\gamma} : (\gamma, \beta).$$

In addition, constraints (A.11)–(A.17) in the Appendix are formulated to ensure the EVs adhere to the scheduling plan obtained for the ITS/SCS automated systems. Accordingly, this model includes constraints that limit the SOC level of the EVs, active power limits for EVs, exclusive charging and discharging actions, CP capability and connection maintenance, and capacity control for charging demand and the power injected into the grid during EV discharge operations.

3.2.3 | Modern power distribution network operational constraints

After an extended period of outage, the cold load pickup (CLPU) phenomenon may occur [44]. To evaluate this, it is necessary to consider the diversified load (P_L^{DI}) and the undiversified load (P_L^U). The CLPU constraint for active and reactive power is formulated in constraints (19) and (20), according to [43, 45]:

$$P_{l,\phi,t}^L = x_{l,\phi,t}^L P_{l,\phi,t}^{DI} + \left(x_{l,\phi,t}^L - x_{l,\phi,t-1}^L \right) P_{l,\phi,t}^U, \quad (19)$$

$$\forall \phi \in \Phi, l \in \mathcal{L}, t \in \mathcal{T},$$

$$Q_{l,\phi,t}^L = x_{l,\phi,t}^L Q_{l,\phi,t}^{DI} + \left(x_{l,\phi,t}^L - x_{l,\phi,t-1}^L \right) Q_{l,\phi,t}^U, \quad (20)$$

$$\forall \phi \in \Phi, i \in \mathcal{L}, t \in \mathcal{T}.$$

When designing a modern power distribution network, the set of switchable loads (\mathcal{L}^S) and non-switchable loads ($\mathcal{L}/\mathcal{L}^S$) must be modelled. A non-switchable load (l) is energized immediately if connected to an energized node (i) using constraint (21); on the other hand, constraint (22) requires that switchable loads (l) only be energized if connected to an energized node (i). Constraint (23) ensures the loads (\mathcal{L}) are not tripped again after their restoration.

$$x_{i,t}^L = x_{i,t}^N, \forall l \in \mathcal{L}/\{\mathcal{L}^S \cup \mathcal{L}^F\}, \phi \in \Phi, t \in \mathcal{T}, \quad (21)$$

$$x_{i,t}^L \leq x_{i,t}^N, \forall l \in \mathcal{L}^S/\mathcal{L}^F, \phi \in \Phi, t \in \mathcal{T}, \quad (22)$$

$$x_{i,t}^L - x_{i,t-1}^L \geq 0, \forall l \in \mathcal{L}^S, \phi \in \Phi, t \geq t_{pe}, t \in \mathcal{T}. \quad (23)$$

Remotely controlled switches (RCSs) are considered alongside manual switches in the MPDN. Constraint (24) limits the number of switching operations, as expressed by the binary variable ($x_{ij,\phi,t}^{RCS}$). It is equal to 1 if the line switches its status from 0 (off) to 1 (on), or from 1 (on) to 0 (off).

$$x_{ij,\phi,t}^{RCS} \leq |x_{ij,\phi,t}^B - x_{ij,\phi,t-1}^B|, \forall ij \in \mathcal{B}^S, \phi \in \Phi, t \in \mathcal{T}. \quad (24)$$

Also, a fault location, isolation, and service restoration (FLISR) model is integrated and represented in constraints (A.18)–(A.24) in the Appendix. This model is integrated into the second stage to ensure the preservation of safe operational conditions within a MPDN. Moreover, similar to the initial stage of MPDN operational constraints, constraints (A.25)–(A.28) are implemented here primarily for power scheduling purposes. They define the feasible ranges for capacitor reactive power, line active and reactive power, while also ensuring the maintenance of MPDN radiality. Additionally, the optimal power flows for three-phase unbalanced MPDN and node balance equations are also integrated and represented in constraints (A.29)–(A.33) in the Appendix.

4 | SOLUTION METHOD

4.1 | Rolling horizon optimization framework

Obtaining massive data on EVs and CPs and the damage status of MPDN components and roads for all time periods of restoration at $t = 0$ is a challenging task [13]. Hence, a rolling optimization framework is adopted to solve the problem recursively by providing a finite-moving horizon of intervals [46]. The time horizon (\mathcal{T}) is discretized into equal time intervals (Δt), and the problem solved at each interval where $\mathcal{T} = 24$ and $\Delta t = 0.5$ h. Here, the decisions and information given in the first interval are implemented and updated at each (t). The prediction horizon is then shifted forward and the

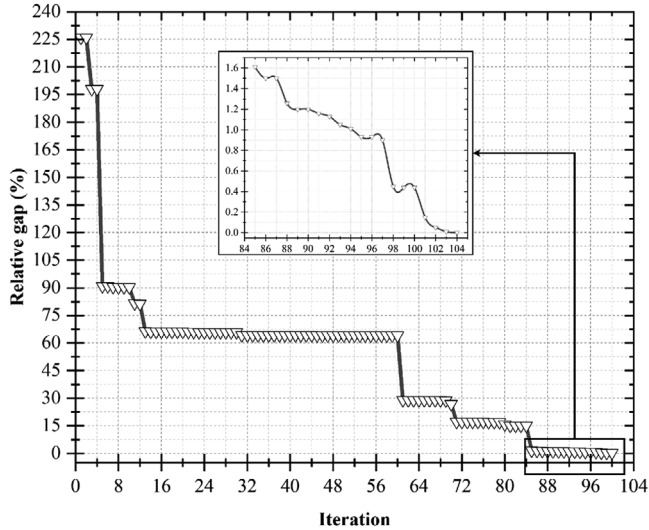


FIGURE 9 The relative optimality gap at each iteration.

calculation repeated at the selected intervals until the end of the time horizon.

4.2 | Linearization techniques

The critical distance calculation model in (10), and the model of energy consumed during travelling in (18) are both non-linear. Therefore, for constraint (10), α is a large parameter used to relax this constraint. The CR variable ($CR_{r,t}^R$) is replaced with a non-constant parameter (CR_r^R), in which the value changes over time for each road. Hence, the distance calculation model in (10) is reformulated and expressed as described by constraints (A.34)–(A.37) in the Appendix. Similarly, the travelling energy consumption model in (18) is non-linear. Thus, it is reformulated and expressed as described by constraints (A.38), which involves eliminating the travelling status variable ($x_{e,t}^{T_e}$) to be maintained in constraint (A.39) as outlined in the Appendix.

5 | SIMULATION STUDIES

5.1 | Intelligent EV coordination performance

The proposed restoration strategy was implemented in the GAMS 42.2.0 studio and solved using Gurobi version 10.0.0 on a PC with a 12th Gen Intel(R) Core(TM) i7-12700k, 3500 MHz CPU processor and 8 GB RAM. The relative optimality gap offers a measure of the difference between primal (z_p) and dual (z_D) objective bounds, and is defined by the incumbent equation (i.e. $gap = |z_p - z_D|/|z_p|$) as per [47]. The gap decreases monotonically until it reaches a threshold of 0.001%, which indicate an optimal solution. This convergence is then demonstrated in Figure 9, where the optimal



FIGURE 10 The map of Battersea road in London, UK, depicting A-, B-, C-roads, as well as all roads combined.



FIGURE 11 The map of Battersea road with different congestion rates (CRs), ranging from high to low level.

strategy is achieved within approximately 40 min at iteration number 104.

5.2 | Test systems

For all three case studies described in Section 6, EVs are considered as viable MPSs suited to the proposed coordination scheme in instances of high penetration of EVs and multiple infrastructures. A UK-wide map of electric car CPs was imported from ZAP-MAP [48], as were real world EV technical characteristics. The repair time for CPs was coupled with MPDN nodes. A map of Battersea road is used to simulate the transportation system, as shown in Figure 10. The roads are categorized as A-, B-, and C-roads, and collected from the UK Government website [49]. CRs are assigned based on Google Maps colour codes representing live traffic speeds, as in Figure 11 [50]. The real distances between T-EVs and the associated CPs are adapted according to real traffic information obtained from Google Maps using a Python client following the model proposed in [51]. The robustness of the proposed framework is verified on a modified three-phase IEEE 123 node test feeder. The repair times for MPDN lines are based on a two-stage stochastic program proposed in [52], which involves dispatching 10 repair crews to repair the damage. The scenario considered involves 15 damaged lines and laterals, as specified in Table 2. Here, the proposed recovery plan in [52] is aligned with the time steps (Δt), which were predefined here. It is further assumed that the MPDN remains separate from the main grid throughout the entire restoration period ($\mathcal{T} = 12$ h). Therefore, the repair time

TABLE 2 The repair times of the damaged lines and laterals [52].

Line	38–39	18–163	58–59	113–114	7–8
Repair time (h)	1.75	1.75	0.5	1.25	2.5
Repair time (Δt)	6	6	6	6	8
Line	54–57	15–17	27–33	105–106	18–19
Repair time (h)	0.75	2.25	2.25	2.75	0.5
Repair time (Δt)	8	10	10	10	12
Line	67–72	76–86	91–93	93–95	150–149
Repair time (h)	5.25	8	1.5	2.75	12
Repair time (Δt)	12	16	16	16	24

for line 150 – 149 is assumed to be 12 h ($\Delta t = 24$) as listed in Table 2.

6 | SIMULATION RESULTS AND DISCUSSION

The application of the proposed MPDN resilience metric enables the evaluation and comparison of different case studies, assessing the effectiveness of novel and advanced framework elements, such as the pre-positioning and dispatching model, information system, integration of ITS/SCS automated system, and geographic graph. These components contribute to achieving an optimal solution managing the geographic and technical data associated with roads, MPDN components, CPs, and EVs. Three case studies are designed as follows:

Case-I: presents the proposed framework.

Case-II: presents a less coordinated approach, wherein the first and second stages are not synchronized, to highlight the robustness of the proposed prepositioning model.

Case-III: presents a non-automated EVs dispatching framework to demonstrate the effectiveness of integrating the proposed information system and geographic graph into MPDN resilience oriented restoration strategies.

The proposed pre-positioning model and constrained large-scale EV routing problem introduce the need for several interrelated decision variables, such as distance travelled by the EVs ($D_{k_q, k_p, e, t}$), energy consumed during travel ($SOC_{e, t}^{tr}$), and the state of charge of the EVs upon arrival at CPs ($SOC_{e, t}^{av}$). The optimal values of these variables influence the MPDN resilience oriented restoration strategy. In Figure 12, the critical path distances ($D_{k_q, k_p, e, t}$), and the median value with the normal distribution curve of ($SOC_{e, t}^{tr}$) are illustrated for each case. Owing to the intelligent preparing stage, the proposed novel prepositioning approach returns significantly lower values for the distance variable ($D_{k_q, k_p, e, t}$) at the early stage of the restoration. This is due to the coordinated efforts of the MPDN operators and automated systems when maximizing $SOC_{e, t}^{av}$ of the EVs, which in turn increases the number of loads surviving ($P_{l, \phi, t}^L$) shortly after a rare event. As time passes, the ITS/SCS automated system updates the decision variables obtained during the first stage. Then, the critical path distance values increase

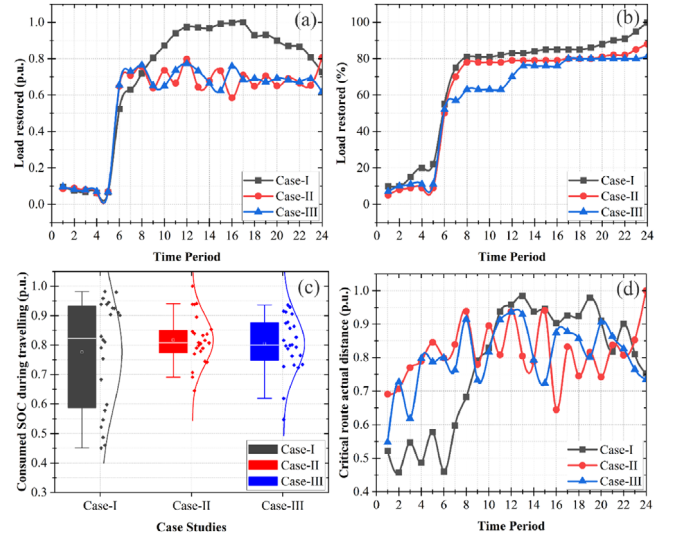


FIGURE 12 The simulation results. (a) The load is restored at each time step ($P_{l, \phi, t}^L$). (b) The cumulative load restored at each time step ($\sum_{l \in T} P_{l, \phi, t}^L$). (c) The median and normal distribution curve for SOC consumed during travel ($SOC_{e, t}^{tr}$). (d) The distance of the critical pathways ($D_{k_q, k_p, e, t}$).

as most of the connected EVs (C-EVs) are discharged (i.e. $SOC_{e, t}^{av} = SOC_{e, t}^L$) and disconnected from the CPs, while the travelling EVs (T-EVs) start their journeys to connect to the CPs for discharge.

Traditionally, the optimal solution typically requires travel over the shortest distance. However, in the case of the proposed approach (Case-I), while it appears to have higher distance values, the ITS/SCS automated systems optimize the distance considering power scheduling constraints, CP utilization, and overloading and queue management at charging stations. The proposed methodology prioritizes the efficient use of CPs and EVs, addressing multiple factors; that is, charging station capacity, battery levels of EVs, and the availability of CPs. This ensures that the optimal charging schedule is achieved without causing a system overload or disruption. Therefore, the proposed BGG optimizes distance in a way that reduces $SOC_{e, t}^{tr}$ achieving a maximum number of restored loads. Thus, Case-I has shown its robustness and resilience; as shown in Figure 12, the median amount of energy consumed during travel ($SOC_{e, t}^{tr}$) in Case-I is the lowest, saving more than 20% ($SOC_{e, t}^{av}$) compared to the other cases.

Moreover, the proposed approach aims to increase ($SOC_{e, t}^{av}$) by maximizing the number of EVs that can be communicated with in both stages. This leads to a higher communication rate among online EVs (i.e. online EVs are those EVs that are can be communicated with via ITS/SCS automated systems through RSUs installed on roads using V2I technology). Thus, around 97%, 86%, and 74% of online EVs can be communicated with in Case-I, Case-II, and Case-III, respectively. This is achieved because the proposed information system allows for efficient collaboration between the automated system of roads and CPs, enabling the continuous transfer and updating of data and decisions obtained constantly. Therefore, the proposed approach achieves a communication rate that is 11%

and 23% higher than Case-II and Case-III, respectively, demonstrating the superiority of the proposed information system for enhancing MPDN resilience.

A high number of communicated EVs is crucial for improving the MPDN resilience, but not all EVs can participate in the restoration process, due to limiting factors such as CP capacity and capability, road CR and status, and the EVs' state of charge levels. Therefore, maximizing the number of participant EVs is a challenging task. Despite this, simulation results indicate the proposed dynamic approach performs well in worst-case scenarios, where 72% of communicated EVs can participate in Case-I. In contrast, only 52% and 17% of EVs participated in Case-II and -III, respectively. This demonstrates the robustness of the proposed approach, which intelligently updates and coordinates between MPDN operators and automated systems, resulting in a 20% and 55% increase compared to Case-II and Case-III, respectively, leading to further enhancement of MPDN resilience.

Figure 12 presents the load restored at each time step, and the cumulative load restored in the presence of the CLPU phenomenon, which can cause delays in the restoration process by absorbing additional power due to undiversified loads ($P_{l,\phi,t}^U$). Case-I, which employs the proposed approach, shows faster and more efficient restoration, with higher objective values at all time steps compared to comparative cases (i.e. Case-II and Case-III). The severe damage scenario assumes the majority of the distribution network's 3-phase lines are damaged at $t = 0$. Nevertheless, the proposed approach still significantly enhances the MPDN resilience by restoring 100% of the load at $t = 24$, which is sooner than in the comparative cases. Specifically, Case-II and Case-III restore around 91% and 81% of the load, respectively, at $t = 24$ indicating more EV (i.e. higher amount of SOC), as well as more time steps, are required to fully restore the MPDN.

Overall, the simulation results in Figure 12 demonstrate the significant impact of the proposed EV coordination framework (Case-I) on the restoration processes. This impact can be attributed to several causes. First, the proposed EV prepositioning model outperforms the comparative case studies by around 20% by leveraging ITS/SCS automated system capabilities to make strategic EV positioning decisions, thereby maximizing the number of loads surviving the early stages of restoration. Moreover, the proposed information system improves the effectiveness of data exchange between entities and EV users, resulting in 23% more participant EVs, increasing the energy injection back into the grid ($SOC_{e,t}^{av}$). This leads to a greater volume of survived and restored loads ($P_{l,\phi,t}^L$), where the amount of load restored at most time steps is higher in Case-I. Additionally, the integration of the proposed BGG exhibits robustness when optimizing routes for a large penetration of EVs, by considering the variations in traffic conditions. This is evident in the lower values for $SOC_{e,t}^{tr}$, despite the higher travel distances observed, as 20% more of EVs energy are preserved. Finally, the results depicted in Figure 12 provide evidence of the enhanced resilience of the MPDN, as demonstrated by the higher objective values achieved with the proposed methodology (Case-I).

In Case-I, the first stage objective value, representing the total load survived, is 3609 kW, while the second stage objective value, representing the total load restored, is 63624.31 kW. In comparison, the comparative case studies (Case-II and Case-III) yield lower objective values. Specifically, Case-II achieves 2790.35 kW for the first stage and 56449.13 kW for the second stage, while Case-III achieves 2412.64 kW for the first stage and 45494.62 kW for the second stage. These findings highlight the effectiveness of the proposed methodology with regard to improving the overall resilience of the MPDN.

7 | SENSITIVITY ANALYSIS AND VALIDATION

The effectiveness of the models proposed here are presented and discussed in separate subsections, with each subsection highlighting the significance of the contributions presented. Section 7.1 assesses and compares the robustness of the pre-positioning and dispatching strategy presented in this study, with the coordination framework proposed in a recently published work. Section 7.2 shows the effectiveness of the proposed information system and its impact on EV coordination strategies, emphasizing its significance in improving coordination efforts of ITS/SCS automated system. In Section 7.3, the effectiveness of the proposed BGG is demonstrated. A sensitivity analysis is conducted with the proposed routing model in recently published works, highlighting the distinctive mechanism of the proposed BGG and its impact on routing decisions.

7.1 | The proposed two-stage optimization approach

The proposed framework is one of the few two-stage optimization frameworks to include a pre-positioning model for MPSs in the first stage and a dispatching model in the second stage. It also focuses solely on the use of MPSs to enhance the resilience of MPDNs and can be compared to that proposed in [23]. While recent works, such as [53, 54], propose similar approaches to enhance MPDN resilience, they extend the concept by incorporating additional factors such as renewable energy sources and repair crews. Such extensions are beyond the scope of the proposed framework. Therefore, comparing the proposed framework to these works may lead to unreliable or misleading findings.

By comparing the proposed framework with [23], the overall effectiveness and performance of the proposed approach can be evaluated. This comparison allows for the identification of the superiority of the proposed framework over existing similar frameworks. To maintain consistency and facilitate effective comparison, the test systems, scenarios, and initial settings are set according to the specifications outlined in [23], with regard to the IEEE-123 node test system, as demonstrated in Figure A1 in the Appendix. The comparison is conducted with the inclusion of six MPSs considering two MESSs with 500

kW/776 kWh capacity, two EV fleet with 150 kW/150 kWh capacity and 0.25 kWh/km energy consumption rate, and two MEGs with 800 kW/600 kVar capacity. The depots and CPs for the associated power sources are also illustrated in Figure A1 in the Appendix, which includes six CPs. Also, the time window for the simulations is modified to $\mathcal{T} = 48\Delta t$, which is equivalent to 24 h with $\Delta t = 0.5$ h. Additionally, the MEGs involved are assumed to be three-phase. The MEGs' operational constraints are also maintained using Equations (A.40) and (A.41) in the Appendix. The MESS operational constraints are also maintained using Equations (A.42)–(A.45) in the Appendix. To simulate the travel in MPSs between depots and CPs, the seismic transportation network presented in [23] is also deployed for all the case studies in this section, to ensure a direct comparison. Accordingly, the two case studies are as follows:

Case-IV: depicts the proposed two-stage optimization framework proposed here.

Case-V: depicts the two-stage optimization framework proposed in [23].

During the prepositioning stage, the proposed approach demonstrates superior performance relative to Case-V, with an approximately 25% increase in the number of survived loads. This improvement is attributed to the integration of the information system into the proposed prepositioning model. By leveraging the capabilities of the ITS/SCS automated system, enhanced prepositioning decisions are made to strategically position the EVs to maximize the number of survived loads during the early stages of the restoration process (from $t = 1$ to $t = 4$). The ITS/SCS automated system utilizes the available shared information on DDCs to effectively preposition EVs, aiming to optimize the utilization of CPs shortly after the event. As a result, the proposed approach achieves higher objective value by ensuring a greater number of loads to survive, and by providing a more efficient and effective restoration process.

In the restorative state, the routing and dispatching strategy proposed in [23] restored more loads between $t = 5$ and $t = 24$, due to the assumption of normal road status, neglecting congestion level, as indicated in Figure 13. In contrast, the proposed strategy accounts for high CRs and severe critical path damage, resulting in longer travel times and distances for some EV fleets and MESS units. Note that, the detailed routing model is discussed in Section 7.3. As a result, the proposed strategy produced lower objective values in the early stages of the restoration process. Nevertheless, the proposed approach outperforms the comparison approach from $t = 25$ onward, as the automated ITS reported the roads as repaired. This update is facilitated by the integration of the proposed information system and BGG. This allows constant updates of road CRs and damage status, resulting in more efficient routing decisions. Thus, higher objective values are observed in Figure 13, as the proposed method exhibits enhanced MPDN resiliency during the post-event state ($t_{pe} \sim t_{pr}$), with a 14% increase in the number of loads survived compared to the case in [23]. This is attributed to the well-coordinated efforts of the operators in the pre-event stage ($t_0 \sim t_{pe}$), as the information generated by the automated systems can be optimally utilized to solve the pre-positioning, routing and power scheduling problems.

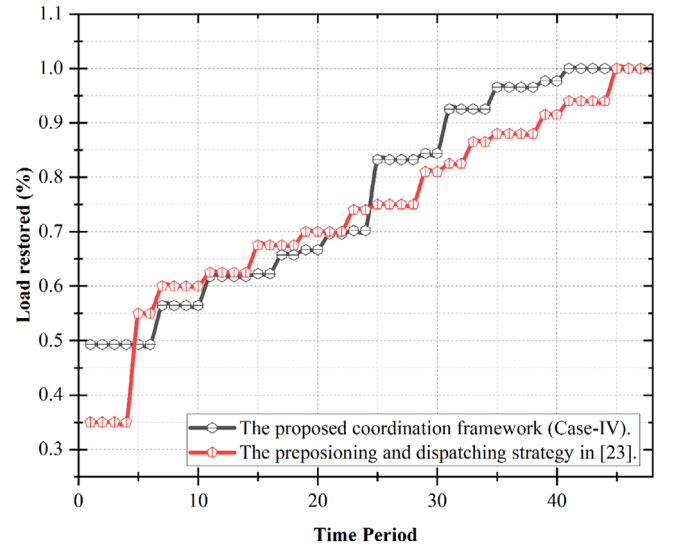


FIGURE 13 Restored loads at each time period for the proposed strategy (i.e. Case-IV) and in [23] (i.e. Case-V).

Overall, the integration of the BGG and information system into the proposed EV coordination approach effectively improves resilience and expedites the restoration of the MPDN. By optimizing the routing and power scheduling of MPSs, the proposed approach enhances overall MPDN resilience and accelerates the restoration process. Consequently, the proposed approach suggests improved resilience with 2 h faster recovery times compared to the approach proposed in [23], thereby maximizing the use of available resources. This enhanced utilization of resources allows for accelerated load restoration efforts. In Case-IV (i.e. the proposed approach), full load restoration is achieved at $t = 41$, which is earlier than the time frame $t = 45$ achieved in [23].

7.2 | The proposed information system

This section conducts comprehensive analysis and evaluation of the proposed information system and its impact on the EV coordination framework. The travelling time, waiting time, and discharging time of the EVs involved in the different case studies are evaluated to highlight the significance of integrating the proposed information system for EV coordination. Furthermore, the length of time a CP (cp) is not operating for discharging (t_{cp}^{nu}) is introduced and calculated as follows:

$$t_{cp}^{nu} = t_e^{cn} - t_e^{deb} - t_{e-1}^{disc}, \forall e \in \check{Y} \subset \mathcal{K}, t \in \mathcal{T}. \quad (25)$$

The sensitivity analysis conducted in this section assesses the effectiveness of the proposed information system designed to coordinate EVs and improve their scheduling and allocation to CPs. Since no similar works or methodologies were identified in the existing literature for comparison, two case studies were designed to validate the proposed methodology. These case studies demonstrate the impact of the proposed

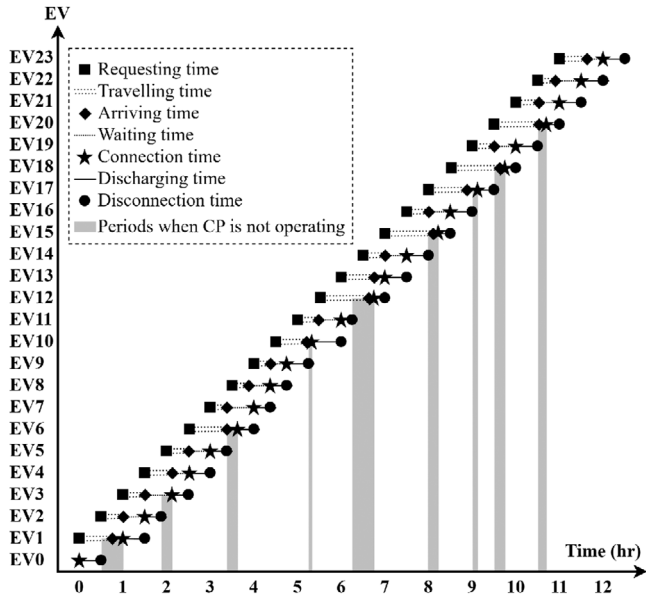


FIGURE 14 The simulation results for the proposed communication methodology (i.e. Case-VI). The vertical axis represents the order of electric vehicle (EV) connections, while the horizontal axis represents time in hours.

communication methodology on the coordination of EVs. The case studies are as follows:

Case-VI: presents the EV coordination results from the requesting time to the disconnecting time, considering both *Task 1* and *Task 2* of the proposed information system.

Case-VII: presents the EV coordination results from the requesting time to the disconnecting time, considering only *Task 2* of the proposed information system.

Here, the proposed EV coordination framework involves more than 90 CPs, making it impractical to demonstrate the detailed coordination results for all the CPs involved individually, therefore, Figure 14 illustrates the results associated with a representative CP. The analysis shows that the CP is not operating (t_{cp}^{nu}) for a duration of approximately 1.5 h, which accounts for 13% of the total restoration period of 12 h. This indicates that the proposed methodology effectively coordinates the EVs, ensuring the CPs are utilized for discharge mainly during the restoration period. Specifically, the total discharging time ($P_{cp,t}^{discb}$) amounts to approximately 87% of the total restoration period. Note that this paper focuses on the effects of the length of waiting time in terms of time, rather than cost of waiting, as the latter is beyond its scope. However, the effects of waiting on restoration processes are thoroughly evaluated in this section. The energy consumption of EVs during waiting is determined to be negligible, as it is typically less than 0.4 kWh per hour of waiting time. This is because EVs are typically in a low-power state when waiting [55].

To further validate the benefits of the proposed information system on MPDN resilience, the results for both cases are listed in Table 3. In this table, the total travelling time (t_e^{tr}) and total waiting time (t_e^w) for the involved EVs are measured in hours (h). The total discharging time (t_e^{disc}) for the EVs and total time when the representative CP is not operating (t_{cp}^{nu}) are measured

TABLE 3 The simulation results of Case-VI and Case-VII considering one representative charging point (CP).

Case	t_e^{tr} (h)	t_e^w (h)	t_e^{disc} (%)	$t_{cp,t}^{nu}$ (%)	Total EVs
Case-VI	4.91	7.21	86.81	13.19	24
Case-VII	5.69	8.34	68.13	31.87	21

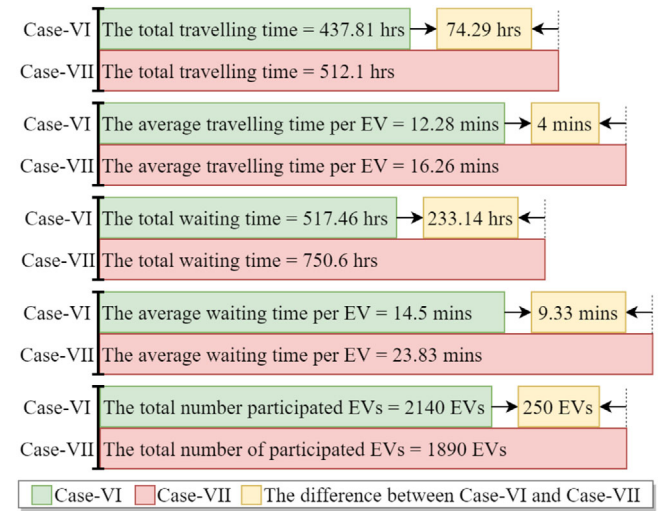


FIGURE 15 The simulation results for Case-VI and Case-VII considering all involved charging points (CPs) and electric vehicles (EVs).

by percentage (%) of the total restoration period ($\mathcal{T} = 12$ h). During the travelling stage, the total travelling time (t_e^{tr}) for 21 EVs in Case-VII is approximately 1 h longer than in Case-VI, which involves 24 EVs. More specifically, the average travelling time for the EVs in Case-VI is around 12 min, while in Case-VII, it is approximately 14 min. The longer travelling time in Case-VII corresponds to a higher cumulative energy consumption value ($SOC_{e,t}^{tr}$) compared to Case-VI, where the information system is fully integrated. This increased $SOC_{e,t}^{tr}$ has a negative impact on the restoration strategy, resulting in a lower amount of total load being restored, as reflected in Figure 12. In the proposed framework, which involves approximately 2000 EVs, this 2-min average increase for each EV results in a travel time that is approximately 67 h longer overall for all the associated EVs, as detailed in Figure 15. This leads to a 723.6 kWh higher energy consumption rate ($SOC_{e,t}^{tr}$) during travel in Case-VII than in Case-VI.

Similarly, in terms of the waiting time (t_e^w), Case-VI outperforms Case-VII. In Case-VI, the average waiting time for each EV is approximately 18 min, which is around 6 min lower than in Case-VII. Additionally, the longer average wait time for each EV at CP, which exceeded 20 min in Case-VI, may have a substantial influence on EV users' decision to participate. It appears likely that EV users are unlikely to participate in scenarios with such long waiting times. Cumulatively, when considering the total number of EVs involved in the proposed EV coordination framework, the total waiting time in Case-VI is approximately 233 h higher than in Case-VII, as indicated in Figure 15. This

higher waiting time significantly impacts the restoration strategy. Moreover, during the waiting period at the involved CPs, the energy consumption rate ($SOC_{e,t}^{tr}$) is higher in Case-VII than in Case-VI where the information system is fully integrated.

Furthermore, in Case-VI, the total discharging period (t_e^{disc}) at the representative CP accounts for the majority of the restoration period (\mathcal{T}). As shown in Table 3, the CP operates discharge mode for approximately 87% of the restoration period, leaving only around 13% of time where the CP is available. The under-utilization of the representative CP during the restoration period in Case-VII is primarily attributed to the absence of the proposed information system. In this scenario, this factor restricts the efficient utilization of CPs, roads, and EVs. It results in under-utilization of the CPs, potentially longer waiting times for EVs, and a fewer EVs participating in the restoration processes, as shown in Table 3 and Figure 15.

Overall, the integration of the proposed information system significantly improves the routing plan, reducing the overall travel time by 14.51% and total energy consumption during EV travel by 19.8%. Furthermore, the total waiting time is reduced by 31.1%, raising the participation rate of EV users by 11.7%. These benefits extend to MPDN operators and ITS/SCS automated systems, enhancing the opportunities for allocation and scheduling of EVs to CPs. As a result, the CPs were able to operate in the discharging mode for more than 87% of the restoration time horizon, effectively enhancing the resilience of the MPDN.

7.3 | The proposed bidirectional geographic graph

This section conducts a comprehensive analysis and evaluation of the proposed BGG and its impact on the EV routing model. The primary objective of the BGG was to facilitate independent travel plans for more than 2000 EVs and 90 CPs within the proposed EV coordination framework. To validate the capabilities of the BGG on the proposed spatial–temporal routing model, an additional set of four case studies were conducted. Thus, this analysis offers clear insights into the impact of the proposed BGG on MPSs routing flexibility and overall resilience. The conducted case studies reflect and evaluate the routing methodology proposed in recently published works [23, 53], and are:

Case-VIII: depicts the proposed routing model here.

Case-IX: depicts the routing model proposed in [23].

Case-X: depicts the routing model proposed in [53].

The simulation in this section employs the IEEE 123-bus distribution test system along with a simplified road network based on the power distribution test system (consistent with the specifications described in Section 7.1). This ensures consistency and comparability with the simulation setup used in [23, 53]. Due to space limitations, the detailed routing decisions set out in the comparative case studies can be found in the original papers [23, 53]. The detailed routing decisions for the proposed routing model are given in Figure 16, where the symbol “→” indicates that a MPS is travelling on the road.

Accordingly, the comparative case studies show that in the earlier stages of the restoration process, travel times are faster, with t being less than $1/2$ of \mathcal{T} . This is because comparative case studies do not consider severe road damage and high CRs. In contrast, the proposed strategy accounts for delays and encounters critical path damage and closures, resulting in longer travel times and distances for some EV fleets and MESS units, as depicted in Figure 16. Specifically, the critical path between CP5 and CP3 was damaged during the event modelled, and was under repair from $t = 13$ to $t = 16$. As a result, EV fleet 1 required approximately four time steps to travel on this road. By contrast, EV fleet 2 only needed one time step as the road had already been repaired. Similar situations occurred for the critical paths between CP5 and CP6, CP3 and CP6, and CP3 and CP4, where roads were damaged and subsequently repaired at different time steps. Additionally, the critical paths between CP1 and CP4, CP1 and CP5, and CP2 and CP6 experienced high CRs, leading to longer total travel times for the corresponding MPSs. This resulted in delays to the routing of MEG1, MEG2, and EV fleet 1, respectively. Once the roads were reported as repaired by the automated ITS at $t = 25$, the BGG demonstrated its effectiveness by incorporating the updated information. This integration enables the dynamic update of road CRs and damage statuses, providing information to generate more accurate and efficient routing decisions. The improved performance resulting from this integration is apparent in Figure 16, where a significant reduction in travel time is evident starting from $t = 25$. This enhanced flexibility in routing mobile power sources on the road network allows for more journeys, surpassing the capabilities of the approaches proposed in [23, 53].

The superior performance of the proposed approach is evident through the higher overall energy usage for load restoration compared to the comparative case studies, as shown in Figure 17. In Case-VIII, the generated power (P^G) represents the total power generated by the involved MPSs shown in Figure 16. However, in Case-X, the generated power includes contributions from MPSs, photovoltaic, and wind turbine sources, as detailed in [53]. Although the precise data for generated power in Case-IX is unavailable in [23], the cumulative load restored is considered equivalent to power generated for comparison purposes. The notable increase in energy utilization achieved by the proposed approach, with 11.21% higher energy usage compared to Case-IX, and 24.93% higher compared to Case-X, contributes to the enhanced resilience of the distribution network.

8 | FURTHER REMARKS

The necessity of separating the stages in the proposed two-stage optimization framework arises from the adverse consequences of combining into a single detailed model. That is, such integration would heighten the complexity and pose computational challenges, diminishing tractability. Moreover, the inter-dependencies between the stages may become complicated, preventing independent analysis and optimization. Hence, it is vital to maintain the separation of stages to ensure a

in overall energy usage for load restoration compared to the comparative case studies. This enhanced energy utilization is achieved through an improved routing plan, resulting in a significant reduction in overall travel times and a substantial decrease in total energy consumption during EV travel. Furthermore, the proposed approach successfully provides more time for CPs to operate in the discharging mode for a significant duration of the restoration time horizon. This enhancement significantly rationalizes the resilience-oriented restoration strategy, as it maximizes the efficient utilization of available power resources throughout the restoration process.

The proposed intelligent framework outperforms all published studies in the literature in worst-case scenarios, by successfully fully restoring loads at a significantly earlier time step. Henceforward, it is crucial for modern power distribution network planners to consider implementing intelligent EV coordination frameworks to enhance resilience-oriented smart restoration strategies as the number of rare events is increasing.

In future work, it is crucial to acknowledge the uncertainties associated with how EV users behave when they are requested to participate in the restoration processes. Authors aims to address these uncertainties technically, and the model addressing this will be presented in another journal paper. Furthermore, the authors have achieved significant progress in addressing the inter-dependencies of MPDN, ITS, and SCS across large areas. This has been accomplished by designing a novel clustering technique along with innovative algorithms, resulting in promising outcomes that surpass commonly employed methods. Additionally, the authors also intend to present this work in an upcoming journal paper.

NOMENCLATURE

Indices

β, ζ	Indices for longitude
γ, δ	Indices for latitude
ϕ	Index for phase number
ρ, ϱ	Indices for two end of the proposed BGG segments
av, tr	Indices for the availability and travelling status
B, N	Indices for line and node
C, O	Indices for capacitor and lines in a loop
cb	Index for the charging status
CP, cp	Indices for CPs
DI, U	Indices for diversified and undiversified load
$disch$	Index for the discharging status
E, e	Indices for EVs
F, S	Indices for faulty, and switchable component
G, g	Indices for MEGs
i, j, ij	Indices for two end nodes and line
L, l	Indices for load
M, m	Indices for MESSs
R, r	Indices for road
RCS	Index for remotely-switchable component
T, t	Indices for time
V, v	Indices for voltage regulator

Parameters

α, M	Large positive numbers
$\eta^{CH/disch}$	The charging/discharging efficiency of the EV battery
$CR_{r,t}$	The congestion rate of road r at time t
ECR_e	The energy consumption rate of EV e

Sets

$\tilde{\mathcal{Y}}$	Set of vertices indicate EV coordinates
$\hat{\mathcal{Y}}$	Set of vertices indicate CP coordinates
\mathcal{H}	Set of the proposed BGG including intersections and edges
\mathcal{K}, \mathcal{E}	Set of intersections and edges of the proposed BGG
\mathcal{N}, \mathcal{B}	Set of nodes and lines
\mathcal{R}, \mathcal{Y}	Set of segments and vertices in a road map
\mathcal{T}, \mathcal{G}	Set of time intervals and EVs
\mathcal{V}, \mathcal{C}	Set of voltage regulators and capacitors
\mathcal{Z}	Set of road map including segments and vertices
Φ, \mathcal{L}	Set of phases and loads

Decision Variables

$\overleftarrow{x}_{k_\varrho, k_\rho, e, t}$	Unidirectional flow variable equals to 1 if an EV e is travelling from k_ρ to k_ϱ at time t
$\overleftrightarrow{x}_{k_\varrho, k_\rho, e, t}$	Bidirectional flow variable equals to 1 if an EV e is either travelling from k_ϱ to k_ρ , or vice versa at time t
$\overrightarrow{x}_{k_\varrho, k_\rho, e, t}$	Unidirectional flow variable equals to 1 if an EV e is travelling from k_ϱ to k_ρ at time t
$D_{k_\varrho, k_\rho, e, t}$	Sum of distance travelled for EV e at time t
$P_{e,t}^{ch/disch}$	The charging/discharging active power for EV e at time t
$P_{m,t}^{ch/disch}$	The charging/discharging active power for MESS m at time t
$Q/P_{g,\phi,t}^G$	The three phase reactive/active power of MEG g for phase ϕ at time t
$Q/P_{i,\phi,t}^N$	The three phase reactive/active power for node i at time t
$Q/P_{l,\phi,t}^{DI}$	The three phase diversified reactive/active power for load l at time t
$Q/P_{l,\phi,t}^L$	The three phase reactive/active power for load l at time t
$Q/P_{l,\phi,t}^U$	The three phase undiversified reactive/active power for load l at time t
$S/Q/P_{ij,\phi,t}^B$	The three phase apparent/reactive/active power of line ij at time t
$SOC_{e,t}^{av}$	Available stat-of-charge level for EV e at time t
$SOC_{e,t}^{tr}$	Consumed stat-of-charge during travelling for EV e at time t
$SOC_{m,t}^{av}$	Available stat-of-charge level for MESS m at time t
$t_{cp,t}^{nu}$	The duration when a CP cp is not operating for discharging

$t_{e,r}^{tr}$	Total travelling time of EV e on road r
t_e^{ar}	The time when an EV e is arrived at the CP
t_e^{cn}	The time when an EV e is connected to the CP
t_e^{dsc}	The duration of discharging time of an EV e
t_e^{dsc}	The time when an EV e is disconnected from the CP
t_e^{rq}	The time when an EV e is requested to participate
t_e^w	The duration of waiting time of an EV e
$V_{i,\phi,t}$	The three phase voltage magnitude for node i at time t
$x_{cp,t}$	Binary variable equals 1 if CP cp is operational at time t
$x_{e,cp,t}$	Binary variable equals 1 if EV e is connected to a CP cp at time t
$x_{e,t}$	Binary variable equals 1 if EV e is connected at time t
$x_{e,t}^{cb/disch}$	Binary variable equals 1 if EV e is charging/discharging at time t
$x_{e,t}^{cb/disch}$	Binary variable equals 1 if electric vehicle e at time t
$x_{e,t}^{tr}$	Binary variable equals 1 if EV e is travelling at time t
$x_{g,\phi,t}^G$	Binary variable equals 1 if MEG g is connected to energized node i and phase ϕ at time t
$x_{g,t}$	Binary variable equals 1 if MEG g is connected at time t
$x_{i,\phi,t}^N$	Binary variable equals 1 if phase ϕ in node i is connected at time t
$x_{ij,\phi,t}^B$	Binary variable equals 1 if phase ϕ in line ij is connected at time t
$x_{ij,\phi,t}^{RCS}$	binary variable equals to 1 if the line ij switches its status from off to on or from on to off.
$x_{l,t}^L$	Binary variable equals 1 if load l is connected at time t
$x_{m,t}$	Binary variable equals 1 if MESS m is connected at time t
$x_{m,t}^{cb/disch}$	Binary variable equals 1 if MESS m is charging/discharging at time t
$x_{v,\phi,t}^V$	Binary variable equals 1 if phase ϕ in line with voltage regulator v is connected at time t

AUTHOR CONTRIBUTIONS

Abdullah Alghamdi: Conceptualization; data curation; formal analysis; investigation; methodology; resources; software; validation; visualization; writing—original draft. Dilan Jayaweera: Conceptualization; methodology; project administration; supervision; writing—review and editing.

ACKNOWLEDGEMENTS

The authors are grateful to the University of Birmingham for funding this research, and also wish to acknowledge the financial support from Taibah University, sponsor of Abdullah Alghamdi. Furthermore, the authors would like to extend their sincere appreciation to the reviewers for their valuable comments and feedback. Their insightful input has also contributed to the improvement and refinement of this work.

CONFLICT OF INTEREST STATEMENT

The authors have declared no conflict of interest.

DATA AVAILABILITY STATEMENT

The data that support the findings of this study are available from the corresponding author upon reasonable request.

ORCID

Abdullah Ali M. Alghamdi  <https://orcid.org/0000-0003-4024-8951>

Dilan Jayaweera  <https://orcid.org/0000-0002-1009-9089>

REFERENCES

1. Alghamdi, A.A.M., Jayaweera, D.: Innovative prepositioning and dispatching schemes of electric vehicles for smart distribution network resiliency and restoration. In: 2022 IEEE PES 14th Asia-Pacific Power and Energy Engineering Conference (APPEEC), pp. 1–6. IEEE (2022)
2. Yuan, W.: Robust optimization-based resilient distribution network planning against natural disasters. IEEE Trans. Smart Grid 7(6), 2817–2826 (2016)
3. Li, Z.: A resilience-oriented two-stage recovery method for power distribution system considering transportation network. Int. J. Electr. Power Energy Syst. 22(135), 107497 (2022)
4. Tran, C.Q.: Stochasticity and environmental cost inclusion for electric vehicles fast-charging facility deployment. Transp. Res. Part E-logistics and Transportation Review. 21(154), 102460 (2021)
5. Hussain, M.T.: Optimal management strategies to solve issues of grid having electric vehicles (ev): a review. J. Storage Mater. 21(33), 102114 (2021)
6. Alghamdi, A.A.M., Jayaweera, D.: Modelling frameworks applied in smart distribution network resiliency and restoration. In: 2022 IEEE 16th International Conference on Compatibility, Power Electronics, and Power Engineering (CPE-POWERENG), pp. 1–8. IEEE, Piscataway, NJ (2022)
7. Zhao, P., Li, C., Fu, Y., Hui, Y., Zhang, Y., Cheng, N.: Blockchain-enabled conditional decentralized vehicular crowdsensing system. IEEE Trans. Intell. Transp. Syst. 23(10), 18937–18950 (2022)
8. Zhang, R., Wu, L., Cao, S., Wu, D., Li, J.: A vehicular task offloading method with eliminating redundant tasks in 5g hetnets. IEEE Trans. Netw. Serv. Manage. 20(1), 456–470 (2022)
9. Wang, X., Garg, S., Lin, H., Kaddoum, G., Hu, J., Hassan, M.M.: Heterogeneous blockchain and ai-driven hierarchical trust evaluation for 5g-enabled intelligent transportation systems. IEEE Trans. Intell. Transp. Syst. 24(2), 2074–2083 (2021)
10. Lei, C., Lu, L., Ouyang, Y.: System of systems model for planning electric vehicle charging infrastructure in intercity transportation networks under emission consideration. IEEE Trans. Intell. Transp. Syst. 23(7), 8103–8113 (2021)
11. Turner, S., Uludag, S.: ‘Towards smart cities: interaction and synergy of the smart grid and intelligent transportation systems’. In: Smart Grid: Networking, Data Management and Business Models, 1 edn, pp. 266–316. CRC Press (2016)
12. Zhu, F., Li, Z., Chen, S., Xiong, G.: Parallel transportation management and control system and its applications in building smart cities. IEEE Trans. Intell. Transp. Syst. 17(6), 1576–1585 (2016)
13. Yao, S., Wang, P., Liu, X., Zhang, H., Zhao, T.: Rolling optimization of mobile energy storage fleets for resilient service restoration. IEEE Trans. Smart Grid 11(2), 1030–1043 (2019)
14. Xu, Y., Wang, Y., He, J., Su, M., Ni, P.: Resilience-oriented distribution system restoration considering mobile emergency resource dispatch in transportation system. IEEE Access 7, 73 899–73 912 (2019)
15. Wang, Y., Xu, Y., Li, J., Li, C., He, J., Liu, J., Zhang, Q.: Dynamic load restoration considering the interdependencies between power distribution systems and urban transportation systems. CSEE J. Power Energy Syst 6(4), 772–781 (2020)
16. Kandaperumal, G., Srivastava, A.K.: Resilience of the electric distribution systems: concepts, classification, assessment, challenges, and research needs. IET Smart Grid 3(2), 133–143 (2020)

17. Hussain, A., Bui, V.-H., Kim, H.-M.: Optimal sizing of battery energy storage system in a fast ev charging station considering power outages. *IEEE Trans. Transp. Electrification* 6(2), 453–463 (2020)
18. Yang, Z., Dehghanian, P., Nazemi, M.: Seismic-resilient electric power distribution systems: harnessing the mobility of power sources. *IEEE Trans. Ind. Appl.* 56(3), 2304–2313 (2020)
19. Jiang, L., Li, X., Long, T., Zhou, R., Jiang, J., Bie, Z., Tian, H., Li, G., Ling, Y.: Resilient service restoration for distribution systems with mobile resources using floyd-based network simplification method: resilient service restoration for ds with mobile resources using floyd-based network simplification method. *IET Gener. Transm. Distrib.* 16(3), 414–429 (2022)
20. Li, B., Chen, Y., Wei, W., Huang, S., Mei, S.: Resilient restoration of distribution systems in coordination with electric bus scheduling. *IEEE Trans. Smart Grid* 12(4), 3314–3325 (2021)
21. Nazemi, M., Dehghanian, P., Yang, Z.: Swift disaster recovery for resilient power grids: integration of ders with mobile power sources. In: 2020 International Conference on Probabilistic Methods Applied to Power Systems (PMAPS), pp. 1–6. IEEE, Piscataway, NJ (2020)
22. Li, B., Chen, Y., Wei, W., Huang, S., Xiong, Y., Mei, S., Hou, Y.: Routing and scheduling of electric buses for resilient restoration of distribution system. *IEEE Trans. Transp. Electrification* 7(4), 2414–2428 (2021)
23. Lei, S., Chen, C., Zhou, H., Hou, Y.: Routing and scheduling of mobile power sources for distribution system resilience enhancement. *IEEE Trans. Smart Grid* 10(5), 5650–5662 (2018)
24. Chang, F.: A coordinated charging strategy for PV-assisted charging station of electric vehicles based on charging service price. In: 2017 IEEE Transportation Electrification Conference and Expo, Asia-Pacific (ITEC Asia-Pacific). IEEE, Piscataway, NJ (2017)
25. Welzel, F.: Grid and user-optimized planning of charging processes of an electric vehicle fleet using a quantitative optimization model. *Appl. Energy* 290, 116717 (2021)
26. Afzal, S., Mokhlis, H., Illias, H.A., Mansor, N.N., Shareef, H.: State-of-the-art review on power system resilience and assessment techniques. *IET Gener. Transm. Distrib.* 14(25), 6107–6121 (2020)
27. Amiroun, M.H., Aminifar, F., Lesani, H.: Towards proactive scheduling of microgrids against extreme floods. *IEEE Trans. Smart Grid* 9(4), 3900–3902 (2017)
28. Drira, W., Ahn, K., Rakha, H., Filali, F.: Development and testing of a 3g/lte adaptive data collection system in vehicular networks. *IEEE Trans. Intell. Transp. Syst.* 17(1), 240–249 (2015)
29. Zeadally, S., Guerrero, J., Contreras, J.: A tutorial survey on vehicle-to-vehicle communications. *Telecommun. Syst.* 73(3), 469–489 (2020)
30. Khan, A.R., Jamlos, M.F., Osman, N., Ishak, M.I., Dzaharudin, F., Yeow, Y.K., Khairi, K.A.: Dsrc technology in vehicle-to-vehicle (V2V) and vehicle-to-infrastructure (V2I) IoT system for intelligent transportation system (ITS): a review. *Recent Trends in Mechatronics Towards Industry 4.0*, pp. 97–106. Springer, Singapore (2022)
31. Lei, S., Chen, C., Li, Y., Hou, Y.: Resilient disaster recovery logistics of distribution systems: co-optimize service restoration with repair crew and mobile power source dispatch. *IEEE Trans. Smart Grid* 10(6), 6187–6202 (2019)
32. Yang, Z., Dehghanian, P., Nazemi, M.: Enhancing seismic resilience of electric power distribution systems with mobile power sources. In: 2019 IEEE Industry Applications Society Annual Meeting, pp. 1–7. IEEE, Piscataway, NJ (2019)
33. Yang, L.-J., Zhao, Y., Wang, C., Gao, P., Hao, J.-H.: Resilience-oriented hierarchical service restoration in distribution system considering microgrids. *IEEE Access* 7, 152 729–152 743 (2019)
34. Ding, T., Wang, Z., Jia, W., Chen, B., Chen, C., Shahidehpour, M.: Multi-period distribution system restoration with routing repair crews, mobile electric vehicles, and soft-open-point networked microgrids. *IEEE Trans. Smart Grid* 11(6), 4795–4808 (2020)
35. Che, L., Shahidehpour, M.: Adaptive formation of microgrids with mobile emergency resources for critical service restoration in extreme conditions. *IEEE Trans. Power Syst.* 34(1), 742–753 (2018)
36. Taheri, B., Safdarian, A., Moeini-Aghataie, M., Lehtonen, M.: Distribution system resilience enhancement via mobile emergency generators. *IEEE Trans. Power Delivery* 36(4), 2308–2319 (2020)
37. Wang, W., Xiong, X., He, Y., Hu, J., Chen, H.: Scheduling of separable mobile energy storage systems with mobile generators and fuel tankers to boost distribution system resilience. *IEEE Trans. Smart Grid* 13(1), 443–457 (2021)
38. Chen, B., Ye, Z., Chen, C., Wang, J.: Toward a milp modeling framework for distribution system restoration. *IEEE Trans. Power Syst.* 34(3), 1749–1760 (2018)
39. Chen, B., Chen, C., Wang, J., Butler-Purry, K.L.: Sequential service restoration for unbalanced distribution systems and microgrids. *IEEE Trans. Power Syst.* 33(2), 1507–1520 (2017)
40. Baran, M.E., Wu, F.F.: Network reconfiguration in distribution systems for loss reduction and load balancing. *IEEE Trans. Power Delivery* 4(2), 1401–1407 (1989)
41. Baran, M., Wu, F.: Optimal capacitor placement on radial distribution systems. *IEEE Trans. Power Delivery* 4(1), 725–734 (1989)
42. Gonçalves, R.R., Franco, J.F., Rider, M.J.: Short-term expansion planning of radial electrical distribution systems using mixed-integer linear programming. *IET Gener. Transm. Distrib.* 9(3), 256–266 (2015)
43. Arif, A., Wang, Z., Wang, J., Chen, C.: Power distribution system outage management with co-optimization of repairs, reconfiguration, and DG dispatch. *IEEE Trans. Smart Grid* 9(5), 4109–4118 (2017)
44. Song, M., Sun, W., et al.: Robust distribution system load restoration with time-dependent cold load pickup. *IEEE Trans. Power Syst.* 36(4), 3204–3215 (2020)
45. Liu, C.-C., Vittal, V., Tomsovic, K., Sun, W., Wang, C., Perez, R., Graf, T., Wells, B., Yuan, H., Moradzadeh, B., et al.: Development and evaluation of system restoration strategies from a blackout-final project report. In: Technical Report PSERC Publication 09-08, Power Systems Engineering Research Center, 577. Engineering Research Center Tempe, AZ (2009)
46. O'Connell, A., Flynn, D., Keane, A.: Rolling multi-period optimization to control electric vehicle charging in distribution networks. *IEEE Trans. Power Syst.* 29(1), 340–348 (2013)
47. 'MIPGap', <https://www.gurobi.com/documentation/9.5/refman/mipgap2.html>. Accessed 17 Jan 2022
48. 'Map of electric charging points for electric cars uk', <https://www.zap-map.com/live>. Accessed 22 Oct 2022
49. 'Statistical gis boundary files for london', <https://www.data.gov.uk>. Accessed 14 Oct 2022
50. 'Map of London', <http://maps.google.co.uk>. Accessed 14 Oct 2022
51. 'Python client library for google maps api web services', <https://github.com/googlemaps/google-maps-services-python>. Accessed 12 Dec 2022
52. Arif, A., Wang, Z., Chen, C., Wang, J.: Repair and resource scheduling in unbalanced distribution systems using neighborhood search. *IEEE Trans. Smart Grid* 11(1), 673–685 (2019)
53. Nazemi, M., Dehghanian, P., Lu, X., Chen, C.: Uncertainty-aware deployment of mobile energy storage systems for distribution grid resilience. *IEEE Trans. Smart Grid* 12(4), 3200–3214 (2021)
54. Li, Z., Tang, W., Lian, X., Chen, X., Zhang, W., Qian, T.: A resilience-oriented two-stage recovery method for power distribution system considering transportation network. *Int. J. Electr. Power Energy Syst.* 135, 107497 (2022)
55. Hussain, S., Kim, Y.-S., Thakur, S., Breslin, J.G.: Optimization of waiting time for electric vehicles using a fuzzy inference system. *IEEE Trans. Intell. Transp. Syst.* 23(9), 15396–15407 (2022)
56. Borghetti, A.: A mixed-integer linear programming approach for the computation of the minimum-losses radial configuration of electrical distribution networks. *IEEE Trans. Power Syst.* 27(3), 1264–1273 (2012)

How to cite this article: Alghamdi, A.A.M., Jayaweera, D.: Resilience of modern power distribution networks with active coordination of EVs and smart restoration. *IET Gener. Transm. Distrib.* , 1–22 (2023). <https://doi.org/10.1049/gtd2.13002>

A.1 | Constraints associated with the EV proactive repositioning model

The following equations pertain to the proposed proactive repositioning model for EVs outlined in Section 3.1. Constraint (A.1) represents the radiality constraint, which is derived from reference [56]. Constraints (A.2) and (A.3) define the limits on the active discharging and charging power of EVs, respectively. Constraint (A.4) ensures the maintenance of appropriate limits to manage the reactive power of a capacitor (v). Constraints (A.5) and (A.6) impose restrictions on line active and reactive power, node voltages, and regulator voltages, to guarantee adherence to safe margins.

$$\sum_{ij} x_{ij,t}^B \leq |B^O| - 1, \forall ij \in B^O, t = 0, \quad (\text{A.1})$$

$$\overline{P}_{e,t}^{discb} x_{e,t} \geq P_{e,t}^{discb} \geq 0, \forall e \in \mathcal{G}^E, t = 0, \quad (\text{A.2})$$

$$\overline{P}_{e,t}^{ch} x_{e,t} \geq P_{e,t}^{ch} \geq 0, \forall e \in \mathcal{G}^E, t = 0, \quad (\text{A.3})$$

$$\overline{Q}_{v,\phi,t}^C x_{v,\phi,t}^V \geq Q_{v,\phi,t}^C \geq 0, \forall v \in \mathcal{V}, \phi \in \Phi, t = 0, \quad (\text{A.4})$$

$$\overline{P}_{ij,\phi,t}^B x_{ij,\phi,t}^B \geq P_{ij,\phi,t}^B \geq \underline{P}_{ij,\phi,t}^B x_{ij,\phi,t}^B, \quad (\text{A.5})$$

$$\forall ij \in \mathcal{B}, \phi \in \Phi, t = 0,$$

$$\overline{Q}_{ij,\phi,t}^B x_{ij,\phi,t}^B \geq Q_{ij,\phi,t}^B \geq \underline{Q}_{ij,\phi,t}^B x_{ij,\phi,t}^B, \quad (\text{A.6})$$

$$\forall ij \in \mathcal{B}, \phi \in \Phi, t = 0.$$

A.2 | Constraints associated with the EV spatial-temporal routing model

The following equations pertain to the proposed spatial-temporal routing model for EVs (i.e. Section 3.2.1). Constraints (A.7)–(A.10) ensure the EVs do not deviate from their routing plan, as initiated by the ITS/SCS automated systems, maintaining start and end intersections, respectively. Constraints (A.7) and (A.8) initiate and conclude the optimal path respectively. Constraint (A.9) ensures the transportation of EVs among different coordinates, satisfying the necessary distance to travel by enforcing the number of incoming and outgoing edges from a node as equal. Constraint (A.10) eliminates sub-tours for the routes and ensures each EV's route follows a single and continuous path that visits all the required coordinates.

$$\sum_{k_\rho} \vec{x}_{k_\rho, k_\rho, e, t} = 0, \forall (k_\rho, k_\rho) \in \mathcal{K}, \quad (\text{A.7})$$

$$(k_\rho, k_\rho) : (\gamma, \beta) = \check{\gamma} : (\gamma, \beta), e \in \mathcal{G}^E, t \in \mathcal{T},$$

$$\sum_{k_\rho} \vec{x}_{k_\rho, k_\rho, e, t} = 1, \forall (k_\rho, k_\rho) \in \mathcal{K}, \quad (\text{A.8})$$

$$(k_\rho, k_\rho) : (\gamma, \beta) = \hat{\gamma} : (\gamma, \beta), e \in \mathcal{G}^E, t \in \mathcal{T},$$

$$\sum_{k_\rho} \vec{x}_{k_\rho, k_\rho, e, t} = \sum_{k_\rho} \overleftarrow{x}_{k_\rho, k_\rho, e, t}, \forall (k_\rho, k_\rho) \in \mathcal{K},$$

$$(k_\rho, k_\rho) : (\gamma, \beta) \neq \check{\gamma} : (\gamma, \beta), k_\rho : (\gamma, \beta) \neq \hat{\gamma} : (\gamma, \beta), \quad (\text{A.9})$$

$$e \in \mathcal{G}^E, t \in \mathcal{T}, t + \tau \leq \mathcal{T}, \tau \leq t_{e,t}^{tr},$$

$$D_{k_\rho, e, t} = 0,$$

$$\forall k_\rho \in \mathcal{K}, k_\rho : (\gamma, \beta) = \check{\gamma} : (\gamma, \beta), e \in \mathcal{G}^E, t \in \mathcal{T}. \quad (\text{A.10})$$

A.3 | Constraints associated with the EV dynamic power scheduling model

The following equations pertain to the proposed dynamic power scheduling model of EVs (i.e. Section 3.2.2). Constraint (A.11) limits the SOC level of EVs within the feasible range. Constraints (A.12) and (A.13) define the active discharging/charging power limits of EVs, respectively. Constraint (A.14) guarantees that charging ($x_{e,t}^{ch}$) and discharging ($x_{e,t}^{discb}$) actions are always mutually exclusive states for each EV (e), and if connected to a CP (cp), it can neither charge nor discharge. It also ensures each EV is positioned and connected at a CP (cp) predetermined by the ITS/SCS automated systems. Constraint (A.15) maintains CP connection capability. Constraints (A.16) and (A.17) maintain CP capacity, where the charging demand and rate of injecting electricity back into the grid do not exceed the capacity of CPs, respectively.

$$\underline{SOC}_{e,t} \leq SOC_{e,t}^{av} \leq \overline{SOC}_{e,t}, \forall e \in \mathcal{G}^E, t \in \mathcal{T}, \quad (\text{A.11})$$

$$\overline{P}_{e,t}^{discb} x_{e,t} \geq P_{e,t}^{discb} \geq 0, \forall e \in \mathcal{G}^E, t \in \mathcal{T}, \quad (\text{A.12})$$

$$\overline{P}_{e,t}^{ch} x_{e,t} \geq P_{e,t}^{ch} \geq 0, \forall e \in \mathcal{G}^E, t \in \mathcal{T}, \quad (\text{A.13})$$

$$x_{e,t}^{ch} + x_{e,t}^{discb} \leq x_{e, cp, t}, \forall e \in \mathcal{G}^E, cp \in \mathcal{N}^{CP}, t \in \mathcal{T}, \quad (\text{A.14})$$

$$\sum_e x_{e,t} \leq x_{cp,t}, \forall e \in \mathcal{G}^E, cp \in \mathcal{N}^{CP}, t \in \mathcal{T}, \quad (\text{A.15})$$

$$0 \leq P_{e,t}^{discb} \leq \overline{P}_{cp,t}^{discb}, \forall e \in \mathcal{G}^E, cp \in \mathcal{N}^{CP}, t \in \mathcal{T}, \quad (\text{A.16})$$

$$0 \leq P_{e,t}^{ch} \leq \overline{P}_{cp,t}^{ch}, \forall e \in \mathcal{G}^E, cp \in \mathcal{N}^{CP}, t \in \mathcal{T}. \quad (\text{A.17})$$

A.4 | Constraints associated with the operation of modern power distribution network

The following equations pertain to MPDN operational constraints (i.e. Section 3.2.3). Constraints (A.18)–(A.24) represent the fault location, isolation, and service restoration (FLISR) model used to reconfigure the MPDN, isolate failed lines, and ensure restored lines cannot be disconnected again [38]. Constraint (A.18) ensures the voltage limits for the MPDN nodes are within the permissible range. Constraint (A.19) forces the MPDN line with voltage regulators to fall within the feasible limits. Constraints (A.20) and (A.21) ensure both end nodes of a switchable line must be energized when activated. Similarly,

constraints (A.22) and (A.23) ensure a non-switchable line is promptly energized when either of its end nodes receives power. Constraint (A.24) establishes that an energized line cannot be tripped afterward.

$$\overline{V}_{i,\phi,t} x_{i,t}^N \geq V_{i,\phi,t} \geq \underline{V}_{i,\phi,t} x_{i,t}^N, \forall i \in \mathcal{N}, \phi \in \Phi, t \in \mathcal{T} \quad (\text{A.18})$$

$$\overline{V}_{ij,\phi,t} x_{ij,t}^B x_{v,t}^V \geq V_{v,\phi,t} \geq \underline{V}_{ij,\phi,t} x_{ij,t}^B x_{v,t}^V, \quad (\text{A.19})$$

$$\forall v \in \mathcal{V}, ij \in \mathcal{B} \cap \mathcal{V}, \phi \in \Phi, t \in \mathcal{T} \\ x_{ij,\phi,t}^B \leq x_{i,\phi,t}^N, \forall ij \in \mathcal{B}^S / \mathcal{B}^F, \phi \in \Phi, t \in \mathcal{T} \quad (\text{A.20})$$

$$x_{ij,\phi,t}^B \leq x_{j,\phi,t}^N, \forall ij \in \mathcal{B}^S / \mathcal{B}^F, \phi \in \Phi, t \in \mathcal{T} \quad (\text{A.21})$$

$$x_{ij,\phi,t}^B = x_{i,\phi,t}^N, \forall ij \in \mathcal{B} / \{\mathcal{B}^S \cup \mathcal{B}^F\}, \\ \phi \in \Phi, t \in \mathcal{T} \quad (\text{A.22})$$

$$x_{ij,\phi,t}^B = x_{j,\phi,t}^N, \forall ij \in \mathcal{B} / \{\mathcal{B}^S \cup \mathcal{B}^F\}, \\ \phi \in \Phi, t \in \mathcal{T} \quad (\text{A.23})$$

$$x_{ij,\phi,t}^B - x_{ij,\phi,t-1}^B \geq 0, \forall ij \in \mathcal{B}^S / \mathcal{B}^F, \phi \in \Phi, 1 \leq t < \mathcal{T} \quad (\text{A.24})$$

Also, constraints (A.25)–(A.33) are utilized primarily for power scheduling purposes, similar to the operational constraints present in the first stage. These constraints define the acceptable ranges for capacitor reactive power (A.25)–(A.27), line active and reactive power (A.27), and the radiality of the modern power distribution network (A.28).

$$\overline{Q}_{v,\phi,t}^C x_{v,\phi,t}^V \geq \underline{Q}_{v,\phi,t}^C \geq 0, \forall v \in \mathcal{V}, \phi \in \Phi, t \in \mathcal{T}, \quad (\text{A.25})$$

$$\overline{P}_{ij,\phi,t}^B x_{ij,\phi,t}^B \geq P_{ij,\phi,t}^B \geq \underline{P}_{ij,\phi,t}^B x_{ij,\phi,t}^B, \\ \forall ij \in \mathcal{B}, \phi \in \Phi, t \in \mathcal{T}, \quad (\text{A.26})$$

$$\overline{Q}_{ij,\phi,t}^B x_{ij,\phi,t}^B \geq \underline{Q}_{ij,\phi,t}^B \geq \underline{Q}_{ij,\phi,t}^B x_{ij,\phi,t}^B, \\ \forall ij \in \mathcal{B}, \phi \in \Phi, t \in \mathcal{T}, \quad (\text{A.27})$$

$$\sum_{ij} x_{ij,t}^B \leq |\mathcal{B}^O| - 1, \forall ij \in \mathcal{B}^O, t \in \mathcal{T}. \quad (\text{A.28})$$

Furthermore, Equations (A.29)–(A.33) are utilized to enforce constraints in the second stage of the three-phase unbalanced MPDN optimal power flow and node balance equations, respectively.

$$V_{i,\phi,t} - V_{j,\phi,t} \leq \tilde{x}_{ij,\phi} S_{ij,\phi,t}^* + \tilde{x}_{ij,\phi}^* S_{ij,\phi,t} \\ + M \left(1 - x_{i,\phi,t}^N \right), \forall ij \in \mathcal{B} / \mathcal{V}, \phi \in \Phi, t \in \mathcal{T}, \quad (\text{A.29})$$

$$V_{i,\phi,t} - V_{j,\phi,t} \geq \tilde{x}_{ij,\phi} S_{ij,\phi,t}^* + \tilde{x}_{ij,\phi}^* S_{ij,\phi,t} \\ - M \left(1 - x_{i,\phi,t}^N \right), \forall ij \in \mathcal{B} / \mathcal{V}, \phi \in \Phi, t \in \mathcal{T}, \quad (\text{A.30})$$

$$\left(\underline{V}_{i,\phi,t} \right)^2 V_{i,\phi,t} \leq V_{j,\phi,t} \leq \left(\overline{V}_{i,\phi,t} \right)^2 V_{i,\phi,t}, \\ \forall i, j \in \mathcal{V}, \phi \in \Phi, t \in \mathcal{T}, \quad (\text{A.31})$$

$$\sum_{ji} P_{ji,\phi,t}^B + P_{e,\phi,t}^{discb} = \sum_{ij} P_{ij,\phi,t}^B + P_{e,\phi,t}^{cb} + P_{l,\phi,t}^L, \\ \forall e \in \mathcal{G}^E, \phi \in \Phi, t \in \mathcal{T}, \quad (\text{A.32})$$

$$\sum_{ji} Q_{ji,\phi,t}^B + Q_{e,\phi,t}^{discb} + Q_{v,\phi,t}^C = \sum_{ij} Q_{ij,\phi,t}^B + Q_{l,\phi,t}^L, \\ \forall e \in \mathcal{G}^E, \phi \in \Phi, v \in \mathcal{V}, t \in \mathcal{T}. \quad (\text{A.33})$$

A.5 | Linear form of the critical distance calculation model

As outlined in Section 4.2, the relaxed form of the non-linear critical distance calculation model in Equation (10) is represented by the subsequent constraints:

$$D_{k_\rho, k_\rho, e, t} = \sum_{k_\rho} x_{k_\rho, k_\rho, e, t} \left(D_{k_\rho, e, t} + \left(D_{k_\rho, k_\rho, e, t} CR_r^R \right) \right), \\ \forall (k_\rho, k_\rho) \in \mathcal{K}, (k_\rho, k_\rho) : (\gamma, \beta) = \check{\gamma} : (\gamma, \beta), \quad (\text{A.34})$$

$$e \in \mathcal{G}^E, t \in \mathcal{T}, t + \tau \leq \mathcal{T}, \tau \leq t_{e,r}^{tr}, r \in \mathcal{E},$$

$$D_{k_\rho, e, t} \leq x_{k_\rho, k_\rho, e, t} \alpha, \forall k_\rho, k_\rho \in \mathcal{K}, e \in \mathcal{G}^E, t \in \mathcal{T}, \quad (\text{A.35})$$

$$D_{k_\rho, e, t} \leq D_{k_\rho, e, t} + D_{k_\rho, k_\rho, e, t}, \quad (\text{A.36})$$

$$\forall k_\rho, k_\rho \in \mathcal{K}, e \in \mathcal{G}^E, r \in \mathcal{E}, t \in \mathcal{T},$$

$$D_{k_\rho, e, t} \geq D_{k_\rho, e, t} + D_{k_\rho, k_\rho, e, t} - \alpha + x_{k_\rho, k_\rho, e, t} \alpha, \\ \forall k_\rho, k_\rho \in \mathcal{K}, e \in \mathcal{G}^E, r \in \mathcal{E}, t \in \mathcal{T}. \quad (\text{A.37})$$

Constraint (A.34) represents the mathematical expression used for calculating the critical distance. To account for all critical roads traversed by an EV (e), constraints (A.35)–(A.37) are implemented. These constraints ensure the distances travelled on critical roads are included in the calculation. To restrict the validity of these constraints to segments associated with critical routes, a large positive number (α) is carefully enforced and selected.

A.6 | Linear form of travelling energy consumption model

As outlined in Section 4.2, a relaxed form of the non-linear travelling energy consumption model in Equation (18) is represented by subsequent constraints, where constraint (A.39) is introduced to enforce EV (e) either in a connection mode (C-EV) or a travelling mode (T-EV).

$$SOC_{e,t}^{tr} = ECR_e D_{k_\varrho, k_\rho, e, t},$$

$$\forall e \in \mathcal{G}^E, k_\varrho, k_\rho \in \mathcal{K}, k_\varrho : (\gamma, \beta) = \check{\gamma} : (\gamma, \beta), \quad (\text{A.38})$$

$$k_\rho : (\gamma, \beta) = \hat{\gamma} : (\gamma, \beta), t \leq t^{ar}$$

$$x_{e,t}^{tr} + x_{e,t} \leq x_{e,cp,t}, \forall e \in \mathcal{G}^E, cp \in \hat{\mathcal{Y}}, t \in \mathcal{T}. \quad (\text{A.39})$$

A.7 | The operational constraints of MEG

Constraints (A.40) and (A.41) play a critical role in ensuring the secure operation of MEGs through the specification of acceptable power ranges. In constraint (A.40), the MEG active power ($P_{g,\phi,t}^G$) is restricted within predefined maximum ($\overline{P}_{g,\phi,t}^G$) and minimum ($\underline{P}_{g,\phi,t}^G$) bounds. Similarly, in constraint (A.41), the reactive power of the MEGs ($Q_{g,\phi,t}^G$) is also ensured to remain within permissible limits. The binary variable ($x_{g,t}^G$) represents the connection status of the MEG. This variable ensures a MEG can only be connected if its terminal node ($g \in \mathcal{G}^G \subseteq \mathcal{N}$) is energized.

$$\underline{P}_{g,\phi,t}^G x_{g,\phi,t}^G \leq \sum_{\phi} P_{g,\phi,t}^G \leq \overline{P}_{g,\phi,t}^G x_{g,t}^G, \quad (\text{A.40})$$

$$\forall g \in \mathcal{G}^G, \phi \in \Phi, t \in \mathcal{T},$$

$$\underline{Q}_{g,\phi,t}^G x_{g,\phi,t}^G \leq \sum_{\phi} Q_{g,\phi,t}^G \leq \overline{Q}_{g,\phi,t}^G x_{g,t}^G, \quad (\text{A.41})$$

$$\forall g \in \mathcal{G}^G, \phi \in \Phi, t \in \mathcal{T}.$$

A.8 | The operational constraints of MESSs

Constraint (A.42) limits the SOC level of MESS within the feasible range, respectively. Constraints (A.43) and (A.44) define the active discharging/charging power limitations of MESSs, respectively. Constraint (A.45) guarantees that charging ($x_{e,t}^{cb}$) and discharging ($x_{e,t}^{disch}$) actions are always mutually exclusive

states for each MESS (e), and if it is not connected to a CP (cp) can neither charge nor discharge. Additionally, it ensures each MESS is positioned and connected to a CP (cp) that is predetermined by ITS/SCS automated systems.

$$\underline{SOC}_{m,t} \leq SOC_{m,t}^{av} \leq \overline{SOC}_{m,t}, \forall m \in \mathcal{G}^M, t \in \mathcal{T}, \quad (\text{A.42})$$

$$\overline{P}_{m,t}^{disch} x_{m,t} \geq P_{m,t}^{disch} \geq 0, \forall m \in \mathcal{G}^M, t \in \mathcal{T}, \quad (\text{A.43})$$

$$\overline{P}_{m,t}^{cb} x_{m,t} \geq P_{m,t}^{cb} \geq 0, \forall m \in \mathcal{G}^M, t \in \mathcal{T}, \quad (\text{A.44})$$

$$x_{m,t}^{cb} + x_{m,t}^{disch} \leq x_{m,cp,t}, \forall e \in \mathcal{G}^M, cp \in \mathcal{N}^{CP}, t \in \mathcal{T}. \quad (\text{A.45})$$

A.9 | Layout of the test system utilised for sensitivity and validation analysis

Figure A1 illustrates the IEEE 123-node test system with MESS stations and charging stations.

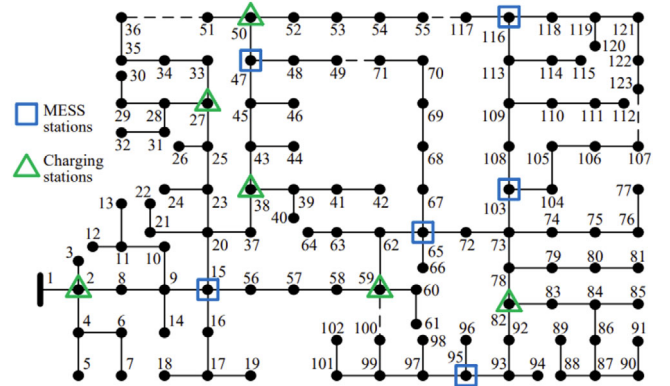


FIGURE A1 Illustration of the IEEE 123-node test system with mobile energy storage system (MESS) stations (i.e. depots) and charging stations (i.e. charging points, CPs). Adapted from the electronic Appendix of [23] for comparison purposes.